Actomyosin Contractility is a Potent Suppressor of Mesoderm Induction by Human Pluripotent Stem Cells

Loic Fort[1,3], Wenjun Wang[2], and Ian Macara[1,3]

[1] Dept of Cell and Developmental Biology, Vanderbilt University School of Medicine Nashville TN 37240 USA

[2] Dept of Biomedical Engineering, Vanderbilt University Nashville TN 37240 USA

[3] Authors for correspondence

Abstract

The activation of WNT signaling in human pluripotent stem cells drives efficient conversion to lateral mesoderm, which can be further differentiated into cardiomyocytes. Stabilization of the WNT effector β-catenin promotes expression of mesoderm-specifying genes such as Brachyury (encoded by *TBXT*) and Eomesodermin and drives an epithelial-mesenchymal transition (EMT) that occurs at 49-52 hrs post WNT activation. Interestingly, WNT activation also triggers an early contraction of stem cell colonies, with increased myosin light chain (MLC) phosphorylation, resulting in cellular morphological changes. Small molecule inhibitors and genetic approaches were applied to determine if contractility is related to mesoderm differentiation. Contrary to expectation, suppressing contractility accelerated differentiation; Brachyury induction was enhanced, and EMT initiated as early as 24 hrs post WNT activation. Conversely, expression of constitutively active Rho kinase or myosin light chain kinase, to increase contractility, efficiently blocked any induction of mesoderm, and cells fail to undergo EMT. Mechanistically, reduced contractility promoted active β-catenin levels in the cytoplasm and nucleus. We propose that the early contraction of human pluripotent stem cell colonies in response to WNT activation initially delays mesoderm induction by restraining accumulation of active β-catenin, suggesting a role for contractility as a temporal gate.

Introduction

Mechanical forces play major roles at many stages of animal development: Starting as early as embryo compaction at the 8-cell stage[1], forces are crucial through gastrulation and later during tissue morphogenesis. Internal forces are largely generated by acto-myosin contractility, and in epithelia are transmitted across cell boundaries by intercellular junctions, enabling collective organization. Tension is generated by these junctions and by adhesion to the extracellular matrix (ECM). Early embryogenesis is marked by waves of cell fate specification to create the three major lineages, followed by further differentiation, and these events are likely coordinated with changes in physical forces created by the cells, to which they then respond. Mechanistically, however, the connections between cell fate and mechanical force remain unclear.

Human embryonic stem cell (hESC) and induced pluripotent stem cell (hiPSC) colonies can be induced to select the mesoderm lineage and eventually to differentiate into functional cardiomyocytes. Pluripotent stem cells are strongly epithelial and lineage specification relies on an epithelial-to-mesenchymal transition (EMT) that is reminiscent of some aspects of gastrulation. When treated with the morphogen BMP4, hESCs can self-organize into 2D "gastruloids" [2], and if plated on compliant hydrogel surfaces they will form "gastrulation-like" nodes that express Brachyury, a mesoderm marker. Micropatterning and traction stress mapping demonstrated that regions of high tension promote Brachyury expression, through release of β-catenin from the cell junctions and consequent activation of WNT signaling, which is known to be required for mesoderm induction [3].

Mesoderm can also be generated from human pluripotent stem cells by direct WNT pathway activation using the small molecule GSK3β inhibitor Chiron 99021 (hereafter CHIR), which protects β-catenin from degradation. Whether mechanical forces play any role in this pathway to mesoderm induction is unknown. We observed that hiPSCs induced by CHIR to differentiate into mesoderm show colony contraction, increased phospho-MLC (myosin light chain) and increased optical retardance, which is a non-invasive measure of actomyosin contractility. From this correlation between contractility and mesoderm induction, plus prior work on BMP4-driven mesoderm in hESCs, we expected that inhibiting actomyosin activity would block induction. Surprisingly, however, we obtained the opposite result: suppressing MLC phosphorylation using small molecule inhibitors or genetic tools substantially promoted mesoderm induction, while

58 further increasing actomyosin contractility was sufficient to block differentiation and EMT
59 completely. Mechanistically, we found that promoting cell relaxation led to an increase in active
60 β-catenin in the cytoplasm and nucleus.
61
62 **Results**
63 WNT-mediated mesoderm specification increases actomyosin contractility
64 To explore how pluripotent stem cells sense, integrate and respond to physical cues, we
65 first investigated whether differentiating cells experience differential forces along their
66 conversion from hiPSC to mesoderm. hiPSCs were treated with CHIR to stabilize β-catenin and
67 thereby activate the WNT pathway, triggering pluripotency exit and commitment to primitive
68 streak and mesoderm lineages. We noticed that hiPSC colonies showed rapid retraction of their
69 edge following CHIR addition **(Supp. Fig 1A)**, consistent with observations from other groups [4].
70 Having previously reported an essential and permissive role for apoptosis during mesoderm
71 specification [5], we tested whether colony retraction was related to the wave of cell death that
72 occurs following CHIR addition. However, co-treatment with a pan-Caspase inhibitor (Q-VD-
73 OPH) did not affect retraction of colony edges **(Supp. Fig 1A)**, ruling out an effect of cell density
74 and cell death.
75 Commitment to the mesoderm lineage also resulted in thicker epithelial layers,
76 containing taller cells **(Supp. Fig 1B-D)**, suggesting profound morphological changes that are
77 highly dependent on the cellular contractile state. Consistent with the role of nuclei as a
78 mechanosensor [6,7], differentiating cells exhibit significantly smaller nuclear area after 48h of
79 CHIR treatment **(Supp. Fig 1E-F)**. To address the variation of cell density, we correlated each of
80 our nuclear area measurements with the actual cell number **(Supp. Fig 1G)**. As expected,
81 nuclear area negatively correlates with cell density before differentiation. However, we did not
82 find any correlation following CHIR treatment, together suggesting that the smaller nuclear size
83 at 48h of differentiation is unlikely to be related to cell density. While these observations were
84 indirect, they point towards a differential contractile status early in mesoderm commitment,
85 switching from low contractile undifferentiated cells to high contractility. To directly test for
86 higher contractility, differentiating cells were stained for phospho-T18/S19 Myosin Light Chain 2
87 (ppMLC), a key regulator of contractility. Immunofluorescences reveal a gradual increase of
88 ppMLC2 intensity over time, with the formation of supracellular fibers extending across several

89 cells **(Supp. Fig 1H-I)**. Finally, we took advantage of the birefringence property of actin fibers to
90 measure light retardance using quantitative polarization microscopy. Birefringence of a material
91 changes proportionally to the applied strain, providing an orthogonal way to probe for
92 contractile status during mesoderm commitment. Confirming our previous data, retardance
93 values increased during hiPSC-to-mesoderm conversion **(Supp. Fig 1J)**. Specificity of the
94 retardance value as a readout for contractility was tested by incubating undifferentiated hiPSCs
95 with a ROCK inhibitor (Y-27632) to suppress MLC phosphorylation. Together, these data suggest
96 that hiPSC differentiating along the cardiac mesoderm trajectory experience increasing
97 contractile forces mediated by MLC2 activity.
98
99 <u>Inhibition of actomyosin contractility promotes hiPSc and hESC conversion to the mesoderm</u>
100 <u>lineage</u>
101 We hypothesized initially that increased contractility might be required for pluripotent
102 cell to acquire their mesoderm identity. To test this hypothesis, hiPSCs were differentiated in the
103 presence of ROCK inhibitor, Y-27632. We first confirmed that MLC2 phosphorylation was
104 reduced by ROCK inhibition **(Supp. Fig 2A-B)**. Contrary to expectations, however, blocking
105 contractility strongly promoted Brachyury expression, a mesoderm marker (encoded by the
106 *TBXT* gene, also known as *T* gene) **(Fig 1A-B)**. Expression of other key mesoderm (*MESP1* and
107 *TBX6*) and EMT (*SNAI1* and *SNAI2*) genes was also upregulated following Y-27632 treatment **(Fig**
108 **1C-F)**. To rule out an effect for ROCK inhibition on global transcription, we examined expression
109 levels of genes unrelated to mesodermal fate and did not detect any response to decreased
110 contractility, suggesting a specific role of actomyosin contractility in cell fate specification **(Supp.**
111 **Fig 2C)**.
112 Normal hiPSCs synchronously undergo EMT at 49-52hrs post-CHIR addition. Brachyury
113 expression is initially restricted to the colony edges at 24hrs, before broader expression across
114 the colony at later timepoints (**Fig. 1G-H**). However, Y-27632 treatment resulted in markedly
115 accelerated EMT, as shown by loss of the epithelial marker ZO-1 from tight junctions (**Fig. 1G, I**)
116 and increased expression of the mesenchymal marker Slug **(Supp. Fig 2D**), plus more
117 widespread Brachyury expression **(Fig. 1G-H)**. To validate these data, we used a more specific
118 ROCK inhibitor, H-1152, which led to similar decreases in ppMLC2 **(Supp. Fig 2E-F)** and
119 recapitulated the early EMT and higher induction of mesoderm markers **(Supp. Fig 2G-M)**.

120 Importantly, these effects of ROCK inhibition were conserved in hESCs expressing a knock-in T-
121 mNeonGreen fusion [3] **(Fig. 1J-K)** and in wild-type H9 hESCs treated with CHIR. Importantly,
122 there was no effect of reduced contractility on exit from the pluripotency state **(Fig 1L and**
123 **Supp. Fig 2N, P)**.
124 Because apoptosis-mediated ATP release is crucial to enable mesoderm fate
125 specification [5], we probed for PARP cleavage as an apoptosis marker but did not detect any
126 difference following addition of Y-27632 or H-1152 **(Supp. Fig 2L and 2N-O)**. MLC2
127 phosphorylation was previously shown to be spatially regulated by ROCK and Myosin Light
128 Chain Kinase (MLCK) in polarized and non-polarized cells [8,9]. Therefore, we tested the
129 involvement of MLCK by treating cells with ML-7, a potent MLCK inhibitor [10]. ML-7 led to
130 efficient reduction in ppMLC2 **(Fig. 1N-O)** and strongly enhanced Brachyury expression at 48h
131 **(Fig. 1P-Q),** without affecting cell death. Together these data unexpectedly show that
132 pharmacological blockade of MLC2-mediated force generation enhances mesoderm
133 commitment quantitatively and accelerates the EMT required for conversion to cardiac
134 mesoderm.
135
136 <u>Genetic suppression of actomyosin contractility promotes stem cell conversion to the</u>
137 <u>mesoderm lineage</u>
138 To rule out off-target effects of the small molecule inhibitors, we designed a genetic
139 approach to suppress contractility in human cells. Dephosphorylation of ppMLC is mediated by
140 Myosin Light Chain Phosphatase, an heterotrimer composed of a catalytic subunit PP1cβ, a
141 Myosin phosphatase-targeting regulatory subunit (MYPT1) and a protein of unknown function
142 M20 [11,12] (**Fig 2A-B**). Based on previous work describing an optogenetic construct to control
143 actomyosin contractility [13], we created a truncated MYPT1, fused with a nuclear export
144 sequence and a mNG reporter (**Fig 2B**), that is expected to act as a constitutively active mutant
145 and promote MLC2 dephosphorylation. To validate the activity of this new tool, we cloned this
146 construct (referred to as MYPT1^{CA}-NES-mNG) under a doxycycline-inducible promoter and
147 established a stable hiPSC line. Global reduction of ppMLC2 was observed by immunoblot and
148 immunofluorescence after doxycycline addition (**Fig 2C-E**). Strikingly, activating MYPT1^{CA}
149 recapitulated the effects of pharmaceutical inhibition of contractility: differentiating MYPT1^{CA}
150 cells displayed enhanced Brachyury expression (**Fig 2F-J**) and earlier induction of the EMT genes

151 Snail and Slug (**Fig 2F**) following Doxycycline induction, compared to controls. Apoptosis
152 induction was not affected in this system (**Fig 2H**). We conclude that reducing MLC2-driven
153 contractility, using either pharmaceutical or genetic strategies, accelerates mesoderm
154 specification.
155
156 <u>Contractility is a potent inhibitor of mesoderm identity</u>
157 Next, we sought to test if constitutively increased contractility impacts hiPSC-to-mesoderm
158 conversion. We stably expressed constitutively active ROCK2 or MLCK ($ROCK2^{CA}$ and $MLCK^{CA}$)
159 under a Doxycycline inducible promoter with ubiquitous expression of a mVenus reporter.
160 Green transduced cells were mixed with unlabeled WT hiPSCs, pre-treated or not with
161 Doxycycline to turn on $ROCK2^{CA}$ or $MLCK^{CA}$ before starting the differentiation protocol for 72h
162 (**Fig 3A**). We first confirmed that mVenus-positive cells treated with Doxycycline showed signs of
163 higher contractility. In the co-culture set up with $ROCK2^{CA}$/WT or $MLCK^{CA}$/WT cells treated with
164 Doxycycline, mVenus-positive clusters showed strong cortical F-actin and higher ppMLC2
165 staining organized as fibers compared to WT mVenus-negative cells, which show more diffused
166 staining (**Supp. Fig 3A, C**). These data support the idea that mVenus-positive cells experience
167 higher contractility, allowing us to test whether cell fate was affected. $ROCK2^{CA}$/WT co-cultures
168 were treated with water (+ Veh) or Doxycycline (+Dox) and stained for mesoderm (Brachuyry)
169 (**Fig. 3B**), primitive streak (EOMES) (**Fig 3D**) and EMT markers (Slug and ZO-1) **(Fig 3F**). mVenus-
170 positive and negative area were drawn based on the mVenus coverage across each cluster
171 (**Supp. Fig 3B-D**) and percentages of cells expressing each marker were reported. Following
172 Doxycycline induction, mVenus-positive clusters showed a dramatic decrease in mesoderm,
173 primitive streak and mesenchymal markers compared to mVenus-negative cells or Vehicle-
174 treated cells (**Fig. 3C-E-G**). Because we previously showed that MLCK inhibition affects
175 mesoderm commitment the same way as ROCK inhibition (**Fig. 1P-Q**), we sought to address the
176 effect of MLCK-driven contractility on cell identity. Importantly, $MLCK^{CA}$-positive clusters failed
177 to commit to the primitive streak and mesoderm lineage and to trigger the EMT program
178 required for mesoderm identity (**Supp. Fig 3E-G**). These data support the surprising conclusion
179 that constant and pre-mature activation of ROCK/MLCK-mediated contractility prevents
180 mesoderm conversion and EMT and is sufficient to counteract the effect of CHIR.
181

182 Reduced cell contractility promotes nuclear accumulation of stable β-Catenin

183 Mechanistically, we first hypothesized that Hippo signaling, one of the main mechanosensitive
184 pathways in epithelial tissues, drives mesoderm specification acceleration upon cell relaxation.
185 YAP, a downstream effector of the Hippo pathway, has been previously associated with cell fate
186 patterning in 2D gastruloids [14]. Activation of the Hippo pathway leads to phosphorylation of YAP
187 at Ser127, restricting its localization to the cytosol and promoting degradation. In contrast, non-
188 phosphorylated YAP translocates to the nucleus and forms a complex with co-transcriptional
189 activator TEAD1-4, together regulating gene expression. Surprisingly, however, phosphorylated
190 YAP was not affected during differentiation or by cell relaxation (**Supp. Fig 4 A-B**). We next
191 directly probed for *CTGF* and *CYR61* expression, two well-described YAP target genes. Gene
192 expression strongly decreased during differentiation but was not affected by cellular contractile
193 status (**Supp. Fig 4C**). Together, these data rule out a significant role for the Hippo pathway in
194 the acceleration of mesodermal differentiation following cell relaxation.

195 Next, we investigated the positive feedback loop reported during BMP4-driven
196 mesoderm commitment, which relies on mechanical tension-dependent secretion of canonical
197 WNT ligands [3]. We treated our MYPT1^{CA}-NES-mNG cells with Doxycycline to trigger cell
198 relaxation and probed for canonical and non-canonical WNT ligands. As a positive control,
199 expression of the mesoderm marker *TBX6* was increased in low contractile cells compared to
200 Vehicle-treated control cells. Interestingly, canonical WNT ligand expression (*WNT3A* and
201 *WNT8A*) was strongly upregulated by suppression of contractility, while non-canonical *WNT4*
202 expression was unaffected neither by CHIR treatment nor by the reduction of contractility
203 (**Supp. Fig 4E**). To test whether increased WNT3A/8A expression was responsible for increased
204 mesoderm commitment in low-contractility cells, we blocked WNT ligand processing and
205 secretion using IWP-2 (Porcupine inhibitor). Addition of IWP-2 did not delay mesoderm gene
206 expression in Y-27632-treated cells, suggesting that this pathway does not drive accelerated
207 mesoderm specification (**Supp. Fig 4F**).

208 We then turned our attention to β-catenin, which exists in epithelial cells both as a
209 cytosolic molecule and bound to E-Cadherin at adherens junctions and plays key
210 mechanosensitive functions during development and tissue homeostasis [3,15]. Whether each
211 pool shares common regulatory mechanisms is still debated [16]. In the absence of WNT signaling,
212 cytosolic β-catenin is associated with a destruction complex, where it is phosphorylated at

213 Ser45 by CK1, which primes the protein for subsequent phosphorylation by GSK3β, driving its
214 ubiquitination and degradation. WNT activation disrupts the destruction complex, permitting
215 the accumulation of stable, non-phosphorylated β-catenin. Therefore, non-phospho β-catenin
216 (hereafter "active" β-catenin) signaling can be assessed from the level of non-phosphorylated
217 Ser45. We evaluated active β-catenin shuttling to the nucleus by isolating cytosolic and nuclear
218 fractions from MYPT1^{CA} cells (**Fig 4A**). Purity of each fraction was assessed from enrichment of a
219 nuclear and cytosolic marker, Lamin A/C and GAPDH respectively (**Supp. Fig 4D**). Strikingly,
220 active β-catenin was strongly upregulated in both the cytosolic and the nuclear fractions in low
221 contractile differentiating cells (24h + Dox) (**Fig. 4B, C**). Immunostaining confirmed the
222 enrichment of active β-catenin in the nucleus 24h post differentiation (**Fig. 4D-F**). We validated
223 this observation by imaging endogenous mEGFP-β-catenin in a knock-in line treated with CHIR
224 in either control or low contractile (Y-27632) conditions. First, we noticed cytosolic
225 accumulation of mEGFP-β-catenin within 5h of CHIR treatment, regardless of the presence of Y-
226 27632. However, consistent with the immunostaining data, mEGFP-β-catenin later became
227 enriched in the nuclei of cells under low contractile stress (**Supp. Fig 4G-H**). Collectively, these
228 findings suggest that the promotion of β-catenin nuclear accumulation by cytoskeletal
229 relaxation accelerates mesoderm program. However, this model can only hold true if the
230 concentration of CHIR used in our study (7.5 μM) does not saturate the β-catenin signaling
231 response. To test this premise, we doubled the concentration of CHIR and probed for expression
232 of WNT target genes as a read-out for WNT signaling (**Fig. 4G**). *LEF1* and *AXIN2* expression
233 responded in a dose-dependent manner to CHIR. Interestingly, however, at any given CHIR
234 concentration, inhibition of cell contractility by addition of Y-27632 further enhanced WNT-
235 target gene responses. Together, these results demonstrate that cell relaxation amplifies active
236 β-catenin translocation to the nucleus synergistically with CHIR to enhance mesoderm
237 commitment.
238
239 **Discussion**
240 Synchronization of developmental processes is key to development. Germ layer specification
241 relies on tight spatio-temporal control of genetic programs, which is concomitant to profound
242 morphological changes during gastrulation. Here, we investigated how differentiating cells sense
243 and integrate physical cues. Our data revealed an unexpected role for acto-myosin contractility

244 as a potent inhibitor of the mesoderm lineage. We discovered that low contractility promotes
245 nuclear localization of β-catenin, which correlates with higher and more rapid mesoderm
246 marker expression (**Fig. 4H**). β-catenin exists as two pools, one bound to the adherens junctions
247 through E-cadherin and one cytosolic pool that is central to WNT signaling. The regulation and
248 exchange of β-catenin molecules between these 2 pools remains poorly understood. E-cadherin
249 binding to β-catenin prevents its nuclear translocation and transcriptional co-activator function
250 [17]. SRC-mediated phosphorylation of β-catenin at residue Y654 reduces binding to E-cadherin [18],
251 so one possibility might be that SRC activity is inversely dependent on contractility in
252 pluripotent stem cells. Alternatively, however, Gayrard et al [19] reported a mechanism through
253 which, in migrating cells, SRC-dependent phosphorylation of FAK causes actin remodeling and E-
254 cadherin tension relaxation, resulting in the release and nuclear translocation of β-catenin. In
255 our system, reduced tension leads to β-catenin accumulation in the cytosolic compartment and
256 translocation into the nucleus as observed by cell fractionation and confocal imaging (**Fig. 4B, D**
257 **and Supp. Fig 4G**).
258
259 We note that the response of pluripotent stem cells to changes in contractility and cell-adhesion
260 tension depends strongly on the environment. For example, contrary to our study, mechanical
261 tension has been reported to promote Brachyury expression in Bilateria[20] while in gastrulation-
262 like models of hESC, Muncie et al showed that high cell adhesion tension can promote
263 mesoderm induction[3]. In this study, authors proposed a dual function for mechanical tension:
264 First, BMP4-driven Brachyury expression relies on mechanical stretch of cell junction that
265 triggers a β-catenin-mechanosensitive response by exposing the conserved Y654 residue.
266 Phosphorylation by SRC-family kinase destabilizes junctional β-catenin and initiates its nuclear
267 translocation. A positive feedback loop reinforces mesoderm commitment through increased
268 canonical WNT ligand secretion. These discrepancies may be explained by differences in the
269 differentiation protocol (BMP4 versus CHIR) and possibly by the substrate/micropattern used [21],
270 providing differential biochemical and mechanical inputs. Indeed, our protocol directly activates
271 WNT pathway by inhibition of the destruction complex, in contrast with BMP4 activation.
272 Our pharmacological and genetic data confirm and expand on a previous study using Y-27632 to
273 enhance mesendodermal differentiation [22], while ruling out potential off target effects of the
274 drug. Our study also suggests that cell fate can be modulated by actomyosin contractility. In

275 *Xenopus,* decreased ROCK-dependent actomyosin contractility promotes an ectoderm-to-
276 mesoderm transition, with ectodermal cells adopting mesoderm-like properties [23]. While we
277 have not tested for alternative cell fate following CHIR addition, our differentiation protocol was
278 adapted from Lian et al [24,25] and was not reported to lead to ectodermal identity. Additionally,
279 we note that differentiating cells lose their pluripotency marks, regardless of their contractile
280 status, suggesting that the rate of pluripotency exit is not affected (Supp. Fig 2N, P).
281
282 Alternative mechanisms might also complement this pathway. For instance, a previous study
283 shows that hiPSC epithelial cohesiveness is a crucial barrier for BMP4-signaling activation, by
284 blocking BMP4 diffusion to the basolaterally-localized BMP receptors and restricting Brachyury
285 expression to the colony edge [26]. However, in our system, the use small molecule inhibitor as a
286 differentiating cue eliminates this diffusion barrier problem. Additionally, while we noticed
287 increased canonical WNT ligand expression following cell relaxation, we ruled out a feed-
288 forward loop by blocking WNT ligand secretion (Supp. Fig 4D-E). Finally, we investigated the
289 activity of the Hippo pathway, as one of the main mechanosensitive pathways. Surprisingly
290 however, we did not detect signature of differential activity during mesoderm specification.
291 Unlike other study on several epithelial and non-epithelial cell lines[27], ROCK inhibition did not
292 affect YAP phosphorylation or expression of YAP target genes. One explanation might be that
293 pluripotent stem cells are insensitive to Hippo activation because of their inability to perceive
294 cell-cell interactions as previously reported [28].
295
296 In several in vivo and in vitro models, including ours, initiation of mesoderm commitment
297 correlates with tissue deformation and cell contraction [3,29–32]. In *Drosophila,* contraction of the
298 posterior end of the embryo is mediated by supercellular active myosin II cables reminiscent
299 with our observation in 2D [32]. Higher contractility also leads to deformation of nuclear
300 morphology, as reported by others [30,33]. Therefore, how can we reconciliate this response with
301 the fact that reducing contractility promotes mesoderm identity? We propose a model in which
302 increasing contractility following the first 24h of differentiation dampens the CHIR response so
303 as to temporally synchronize mesoderm identity. Indeed, in the developing embryo,
304 specification of lineages required deep morphological changes and cell compaction, mostly
305 mediated by actomyosin contractility [34–36]. It is widely accepted that high density cells, similar to

306 ingressing cells during gastrulation, have low contractility compared to cells at low density, both
307 in vitro and in vivo [37]. Our work suggests that this mechanical gate prevents mesoderm
308 specification until mechanical tension is released. Inducing low contractility prior to CHIR
309 treatment, disrupts this mechanical gate, resulting to accelerated mesoderm identity and EMT.
310

311 **Limitations of the study**

312 In this study, we aimed to understand if and how mechanical tension is important for mesoderm
313 lineage specification. To this end, we used a simple 2D system, allowing us to control most
314 parameters while only perturbing actomyosin contractility. However, this 2D system is limited in
315 its physiological parallels. Translation of these data into 2.5D and 3D models of gastrulation (2D
316 and 3D gastruloid respectively), and alternatively into early mouse development will test the
317 generalization these findings. Moreover, while we consistently observed higher β-catenin in the
318 nucleus upon cell relaxation, further work will be required to address whether it reflects an
319 increase of import or a decrease of export from the nucleus.
320 Finally, it remains to be addressed whether increased nuclear β-catenin results from increased
321 binding to its target gene promoters, such as the Brachyury promoter, which contains two
322 TCF/LEF-1/β-catenin binding sites within the first 500pb [38,39]. Further work on chromatin
323 rearrangement will be required to better understand whether enhancer/repressor are spatially
324 modulated by mechanical tension.
325

326 **Acknowledgements**

327 We thank Cynthia Reinhart-King for giving us access to the QPOL facility. We thank the Weaver
328 lab (UCSF) and the Gardel lab (University of Chicago) for sharing the T-mNG knock-in hESC line.
329 We also thank all members of the Macara lab, especially Vaishna Vamadevan and Christian de
330 Caestecker for valuable suggestions and advice. This work was funded by an American Heart
331 Association postdoctoral fellowship (Award ID 23POST1018347 to L.F.), a Vanderbilt
332 Mechanobiology fellowship (to L.F.) and a grant from the National Institutes of Health
333 (GM070902 to I.G.M.).
334

335 **Author contributions**

336 L.F. conceived the study, performed and quantified all experiments except the QPOL, and wrote
337 the manuscript. W.W. imaged and quantified the QPOL data. I.G.M. supervised the project, and
338 edited the manuscript
339
340 **Declaration of interest**
341 The authors declare no competing interests.
342
343 **Material & Methods**
344 Research compliance and ethical regulation
345 All experiments using human ESCs were performed using the WA09 (H9) cell line under the
346 supervision of the Vanderbilt Institutional Human Pluripotent Cell Research Oversight
347 Committee (protocol IRB no. 160146). No cells were sourced directly from human embryos.
348
349 Reagents
350 Common laboratory reagents used in this study are listed in Supplementary Table 1
351
352 Cell culture and maintenance
353 Human GM25256 iPSCs were obtained from the Coriell Institute. The mEGFP–CTNNB1 knock-in
354 GM25256 iPSC cell line was obtained from the Allen Cell Collection, Coriell Institute (cell ID
355 AICS-0058-067). The human ESC line H9 (WA09) was obtained from the WiCell Research
356 Institute. The T-mNG knock-in hESC H9 was made by Valerie Weaver lab (UCSF) and kindly
357 provided by Margaret Gardel (University of Chicago). The iPSC and ESC H9 lines were cultured
358 on Matrigel-coated six-well plates (Matrigel diluted at 42 µg ml−1 in DMEM/F12 medium) and
359 cultured in mTeSR1 medium. The medium was changed daily until the cells reached 70%
360 confluency. Cells were passaged using Gentle cell dissociation reagent for 4 min, resuspended in
361 mTseR1 medium as small clusters and replated at 1:7.
362 HEK293T cells were obtained from the ATCC. Cells were grown in 10% FBS DMEM medium and
363 passaged at 1:10 every 2-3 days.
364 All cell lines used in this study were maintained at 37 °C under 5% CO_2.
365
366 Cell freezing and thawing

367 Human iPSCs and ESCs were harvested from culture dishes using Gentle cell dissociation
368 reagent and centrifuged at 120g for 3 min. The pellets were resuspended in mTeSR1 medium
369 supplemented with 10% DMSO and aliquoted into cryovials. Cells were first transferred to
370 −80 °C for 24 h before long-term storage in liquid nitrogen. iPSCs and ESCs were slowly thawed
371 using mTeSR1, centrifuged and resuspended in mTeSR1 supplemented with 10 µM Y-27632 for
372 24 h.
373
374 Mesoderm differentiation protocol
375 Differentiation was initiated when cells reach 70-80% confluency. Cells were treated with 7.5
376 µM CHIR99021 (hereafter CHIR) diluted in RPMI media supplemented with 1X B27 minus insulin
377 and 100U/mL Penicillin and 100 µg/mL streptomycin (1X) for up to 72 hours.
378 For pharmaceutical inhibition of contractility, cells were pre-treated overnight with respective
379 drug or vehicle (water) diluted in mTeSR1. Differentiation was initiated by switching to CHIR
380 media as described above, supplemented with respective drug or vehicle (water). Similarly, cells
381 were pre-induced overnight with Doxycycline or vehicle (water) diluted in mTeSR1 before
382 initiating the differentiation protocol in the presence of Doxycycline or water. For concentration
383 of each drug, please refer to Supplementary Table 1.
384
385 Lentiviral preparation
386 HEK193T were grown at 40% confluency in 10 cm plate and transfected using Calcium-
387 Phosphate. Briefly, 20 µg of lentiviral plasmid, 15 µg of pSPAX2 (Addgene #8454) and 6 µg
388 pMD2G (Addgene #12260) were mixed with 450 µL sterile water and 50 µL of 2.5M $CaCl_2$
389 solution, previously filter sterilized. DNA mixture was added dropwise into 500 µL of 2X HeBS
390 (50 mM HEPES, 10 mM KCl, 12 mM dextrose, 280 mM NaCl and 1.5 mM Na2PO4, pH 7.04) with
391 constant vortexing. Solution was added dropwise on HEK 293T cells for 6h. Medium was
392 replaced with 8mL of fresh 10% FBS DMEM medium for 48h. Supernatant was filtered through a
393 0.22 µm membrane and concentrated using a 100kDa cut-off Amicon centrigal unit. Aliquots
394 were frozen at -80 °C.
395
396 SDS-PAGE and Western blotting

397 Cells were washed with ice cold 1X PBS and lysed with 70 µL RIPA buffer (150 mM NaCl, 10 mM
398 Tris–HCl pH 7.5, 1 mM EDTA, 1% Triton X-100, 0.1% SDS) supplemented with and 1X protease
399 and phosphatase inhibitors. Mechanical disruption was performed by scrapping the cells off the
400 plate, transferring the lysate into a 1.5mL Eppendorff tube and vortexing for 5 seconds followed
401 by 5 min incubation on ice. Soluble proteins were collected by centrifugation at 16000 g (13200
402 rpm) for 10min at 4°C. Protein concentration was measured using Precision Red following the
403 manufacturer's instructions. Lysates in sample buffer were boiled for 5min.
404 For ppMLC blotting, cells were washed with 1X PBS and directly lysed using 250 µL of boiling 1X
405 Sample buffer. Lysates were sonicated 3 times for 10 seconds with 60 seconds incubation on ice
406 between each blast.
407 30 µg of proteins were resolved on 1.5mm thick bis-tris acrylamide gels and transferred onto
408 0.2 µm nitrocellulose membrane using BioRad wet transfer system (50 V for 2hours).
409 Membranes were blocked for > 30min at room temperature (RT) with 5% BSA in 1X TBS-T
410 (10 mM Tris pH 8.0, 150 mM NaCl and 0.5% Tween 20) and incubated overnight at 4°C and
411 gentle rocking with primary antibodies diluted in blocking buffer (Supplementary Table 2).
412 Membranes were washed 3 times with 1X TBS-T and incubated for 1h at RT with AlexaFluor-
413 conjugated secondary antibodies (Supplementary Table 2). After 3 additional washes in 1X TBS-
414 T, membranes were scanned using Li-Cor Odyssey CLx system, analyzed and processed using
415 Image StudioLite v. 5.2.
416
417 <u>Immunofluorescence</u>
418 Cells were cultured on Matrigel-coated Ø 12mm coverglass, fixed with 4% paraformaldehyde for
419 10min, permeabilized for 5min at RT (20mM Glycine, 0.05% Triton X-100 in 1X PBS), and
420 incubated with blocking buffer for > 30min (5% BSA in 1X PBS). Coverslips were transferred into
421 a dark humidified chamber and incubated with primary and AlexaFluor-conjugated secondary
422 antibodies (Supplementary Table 2) diluted in blocking buffer for 2 hours. Coverslips were
423 washed in 1X PBS and mounted on glass slide using Fluoromount-G mounting solution.
424 For ppMLC staining, samples were incubated overnight with primary antibody.
425
426 <u>Image acquisition, analysis and processing</u>

427 Micrographs were obtained using an inverted Nikon A1-R confocal microscope equipped with a
428 x20 objective (Numerical aperture NA 0.75), a x40 oil objective (NA 1.20) and a x100 oil
429 objective (NA 1.40). Z-stacks covering the entire cell height were acquired. Maximum Intensity
430 Projections were obtained and images were analyzed and processed using Fiji (version
431 2.1.0/1.54f).
432
433 MYPT1^{CA}-NES-mNeonGreen cloning strategy
434 gBlock corresponding to truncated human MYPT1 (aa 1-300) was built in fusion with a PKI super
435 NES and mNeonGreen sequence. gBlock was amplified using Fusion polymerase and the
436 following primers: Fwd 5'-CTGCTGACCGGTACCATGGCGGACGCGAAGC-3' and Rev 5'-
437 CATCATACGCGTCTACGATCCGCCACCGC-3'. PCR product and recipient backbone (pInducer10b-
438 HA-KRas G12V Addgene #164928) were digested with AgeI-HF and MluI-HF for 1h at 37°C, gel
439 purified and ligated overnight at 16°C using T4 ligase. Ligation reactions were transformed into
440 chemically competent E.Coli Stbl3 strain by heatshock (45 sec at 42°C) and selected on
441 Ampicillin plate. Clones were isolated and set up for MiniPrep (QIAprep Spin MiniPrep kit). The
442 presence of the insert was confirmed by restriction digest check. Positive clones were sent for
443 full plasmid sequencing provided by Genewiz Plasmid-EZ service before MidiPrep using Takara
444 Bio NucleoBond XtraMidi kit.
445
446 Flow cytometry analysis
447 T-mNeonGreen knock-in hESC were transduced with a lentivector expressing Histone 2B-
448 mScarlet (pWPI-H2B-mScarlet). Cells were pre-treated overnight with Vehicle (water) or 10 µM
449 Y-27632. Differentiation was initiated for 24 hours as described above and cells were harvested
450 as single cells. Briefly, cells were washed and gentle cell dissociation buffer was added for 8 min
451 at 37°C. Cell suspension was centrifuged and resuspended in 500 µL PBS. Cells were passed
452 through a Ø 40 µm strainer directly into 500 µL of 8% PFA (final concentration 4%) and fixed for
453 10 min on a wheel before sending them for cytometry using a 5-laser Fortessa analyzer (70 µm
454 nozzle). Singlets were selected based of forward and side scatter. mScarlet (PE-Texas-RedA) and
455 mNeonGreen (GFP-A) population were selected by drawing a gate on double negative WT hESC
456 shifted by one order of magnitude. Percentage of mNeonGreen/mScarlet double positive was
457 reported.

458

459 RNA isolation and RT-qPCR

460 Cells were washed and RNAs were isolated using RNeasy mini kit following manufacturer's
461 instructions. 1 µg of RNA was reverse transcribed to cDNA using the SuperScript III first-strand
462 synthesis kit. cDNA was diluted 1:5 in water and mixed with Maxima SYBR Green/1mM of each
463 primer (Supplementary Table 3). Quantitative PCR was performed on a BioRad CFX96
464 thermocycler. C_t values from technical triplicates were averaged and normalized to GAPDH using
465 the $\Delta\Delta C_t$ formula.

466

467 Cell Fractionation

468 Following appropriate treatment, cells were washed with ice cold 1X PBS and collected as single
469 cell suspension using gentle cell dissociation as previously described. Cell suspension was
470 washed with cold 1X PBS and resuspended in 500 µL of cold PBS. 100 µL of the cell suspension
471 was set aside and mixed with 30 µL of 4X sample buffer. Sample was sonicated for 15 sec at 20%
472 power 3 times, boiled 5min and stored at -20 °C (Whole Cell Lysate fraction or WCL).
473 Cell fractionation was performed using Cell signaling kit (#9038) and their protocol. Briefly, the
474 remaining 400 µL of cell suspension was centrifuged at 500 x g at 4°C for 5min. Supernatant was
475 removed and pellet was resuspended in 250 µL of CIB buffer, vortexed for 5 sec and incubated
476 on ice for 5 min. Samples were centrifuged at 500 x g at 4°C for 5min and supernatant was
477 stored in pre-chilled tube (= Cytoplasmic fraction). Pellet was resuspended in 250 µL of MIB
478 buffer, vortexed for 15 sec and incubated on ice for 5 min. Samples were centrifuged at 8000 x g
479 at 4°C for 5min and supernatant was discarded (= Membrane and organelle fraction). Pellet was
480 resupended in 125 µL of CyNIB buffer, sonicated for 5 sec at 20% power 3 times (cytoskeletal
481 and nuclear fraction). Each fraction was mixed with the appropriate volume of 4X sample buffer
482 to obtain a final concentration of 1X. Samples were boiled for 5min and centrifuged before
483 loading 15 µL.

484

485 Reproducibility and statistics

486 All datasets were analyzed using GraphPad Prism10 (version 10.0.3). Individual measurements
487 (n) were averaged for each biological repeat (N). Datasets were tested for normality (Shapiro-
488 Wilk test) before applying the appropriate statistical test on the biological repeat (N), except if

489 mentioned differently in the figure legend. For dataset displayed as superplots, individual
490 measurements and biological repeats are represented by small and large dots respectively. Each
491 dataset for a biological repeat is color coded. Error bar represent S.D. Significance levels are
492 given as follows and exact P values are indicated in each figure: NS, not significant ($P \geq 0.05$);
493 *$P < 0.05$; **$P < 0.01$; ***$P < 0.001$; and ****$P < 0.0001$.
494 All experiments, including representative MIPs and western blots, were performed at least three
495 times independently as biological repeats, unless stated otherwise in the legends. No statistical
496 method was used to pre-determine the sample size, the experiments were not randomized and
497 the investigators were not blinded to allocation during experiments and outcome assessment.
498
499 **Figure legends**
500 Figure 1: Pharmaceutical inhibition of actomyosin contractility promotes hiPSc and hESC
501 conversion to the mesoderm lineage
502 A, B – Immunoblot of Brachyury during hiPSC-to-mesoderm commitment (0-48h) in the
503 presence (+ Y-27632) or absence (+ Veh) of ROCK inhibitor. Molecular weights (M.W.) are
504 displayed on the right side (A). Brachyury expression was quantified by densitometry and
505 normalized to α-Tubulin as loading control across N=3 independent biological repeats (B). Mean
506 and S.D. are displayed. Two-tailed unpaired t test was performed.
507 C-F – Relative expression of mesoderm markers (*MESP1, TBX6*) (C, D) and EMT markers (*SNAI1,*
508 *SNAI2*) (E, F) 48h post CHIR treatment in the presence (+Y-27) or absence (+Veh) of ROCK
509 inhibitor. N=3 independent biological repeats except for *MESP1* N=4 independent biological
510 repeats. Mean and S.D. are displayed. Two-tailed unpaired t test was performed.
511 G-I – Representative MaxIP immunofluorescences during hiPSC-to-mesoderm commitment (0-
512 48h) in the presence (+ Y-27632) or absence (+ Veh) of ROCK inhibitor. Cells were stained with a
513 nuclear marker (DNA), EMT marker (ZO-1 – Inverted LUT) and Mesoderm marker (T/Bra–
514 Inverted LUT). Scale bar = 50 µm (G). Quantification of Brachyury expression (H) and ZO-1
515 intactness (I) is represented as violin plots with individual measurements (small dots) averaged
516 for each biological repeat (large dots). Median (Plain red line) and quartiles (Dotted black lines).
517 n=10-15 technical repeats across N=3 independent biological repeats. One-way ANOVA with
518 Tukey's multiple comparisons post-test was performed on biological repeats.

519 J, K – Analysis of Brachyury expression by flow cytometry following 24h CHIR treatment in the
520 presence (+Y-27632) or absence (+Veh) of ROCK inhibitor using Bra-mNeonGreen knock-in H9
521 hESC line (J). Quantification of the percentage of cells mNeonGreen-positive from N=4
522 independent biological repeats. Mean and S.D. are displayed. Two-tailed unpaired t test was
523 performed (K).
524 L, M – Immunoblot of Brachyury (mesoderm) and Nanog (Pluripotency marker) using hESC H9 in
525 the presence (+ Y-27632) or absence (+ Veh) of ROCK inhibitor. Molecular weights (M.W.) are
526 displayed on the right side (L). Brachyury expression was quantified by densitometry and
527 normalized to α-Tubulin as loading control across N=3 independent biological repeats (M).
528 Mean and S.D. are displayed. Two-tailed unpaired t test was performed.
529 N, O – Representative MaxIP immunofluorescence of hiPSCs treated with a MLCK inhibitor (ML-
530 7) or Vehicle (DMSO) and stained for nuclei (DNA) and phospho T18/S19 Myosin Light Chain 2
531 (ppMLC2 – Inverted LUT). Scale bar = 50 µm. Magnified views of the yellow dotted ROI are
532 shown for ppMLC2. Scale bar = 20 µm (N). Percentage of cellular area positive for ppMLC2
533 following Vehicle or ML-7 treatment is reported as violin pots. Median (Plain red line) and
534 quartiles (Dotted black lines). n=15 technical repeats across N=3 independent biological repeats.
535 Two-tailed unpaired t test was performed on the biological repeats.
536 P, Q - Immunoblot of Brachyury (mesoderm) and PARP (Cell death marker) using hiPSCs in the
537 presence (+ ML-7) or absence (+ Veh) of MLCK inhibitor at basal state (0h) and during CHIR
538 treatment (24h, 48h). Molecular weights (M.W.) are displayed on the right side (P). Brachyury
539 expression was quantified by densitometry and normalized to α-Tubulin as loading control
540 across N=3 independent biological repeats. Mean and S.D. are displayed. Mann-Whitney test
541 was performed for the 24h timepoints and two-tailed unpaired t test was performed for the 48h
542 timepoints (Q).
543
544 <u>Figure 2: Genetic inhibition of actomyosin contractility promotes hiPSc conversion to the</u>
545 <u>mesoderm lineage</u>
546 A – Summary of the main regulators of MLC phosphorylation.
547 B – Schematic representation of full length MYPT1 (1030 aa), interacting with PP1c phosphatase
548 and protein of unknown function M20. Truncation of MYPT1 Cterm Δ301-1030 leads to a

549 constitutive recruitment and activation of PP1C. Truncated MYPT1 was fused with NES-
550 mNeonGreen and is referred to as MYPT1^{CA}-NES-mNG.
551 C – Immunoblot of phospho T18/S19 MLC2 (ppMLC2) and total MLC2 in WT hiPSCs treated with
552 Doxycycline or hiPSC expressing MYPT1^{CA}-NES-mNG in the presence or absence of Doxycycline.
553 α-Tubulin was used as loading control. Molecular weights (M.W.) are displayed on the right side
554 D, E – Representative MaxIP immunofluorescence of hiPSC expressing MYPT1^{CA}-NES-mNG and
555 treated or not with Doxycycline. Cells were fixed and stained for phospho T18/S19 MLC2
556 (ppML2 - Magenta), DNA (blue) and tight junction marker ZO-1 (Orange). Scale bar = 50 µm (D).
557 Fraction of the cellular area positive for ppMLC2 following Doxycycline induction of MYPT1^{CA}-
558 NES-mNG hiPSC and reported as violin plots. Median (Plain red line) and quartiles (Dotted black
559 lines). n=32 technical repeats across N=3 independent biological repeats. Two-tailed unpaired t
560 test was performed on the biological repeats (E).
561 F, G – Representative immunoblot for Brachyury (mesoderm marker), Snail and Slug (EMT
562 markers) using WT and MYPT1^{CA}-NES-mNG hiPSCs, following CHIR treatment (0h-48h) in the
563 presence or absence of Doxycycline. Molecular weights (M.W.) are displayed on the right side
564 (F). Brachyury expression was quantified by densitometry and normalized to α-Tubulin as
565 loading control across N=3-4 independent biological repeats. Mean and S.D. are displayed. A
566 one-way ANOVA with Tukey's multiple comparisons post-test was performed (G).
567 H – Immunoblot of PARP (cell death marker) and Brachyury (Mesoderm marker) during
568 mesoderm commitment (0h-48h CHIR) using MYPT1^{CA}-NES-mNG hiPSCs induced with
569 Doxycycline. Molecular weights (M.W.) are displayed on the right side.
570 I, J – Representative MaxIP immunofluorescences of WT and MYPT1^{CA}-NES-mNG hiPSCs treated
571 with CHIR for 24h +/- Doxycycline. Cells were stained for nuclei (DNA), EMT marker (ZO-1 –
572 Inverted LUT) and Mesoderm marker (T/Bra – Inverted LUT). Scale bar = 100 µm (I).
573 Quantification of Brachyury expression is presented as violin plots. Median (Plain red line) and
574 quartiles (Dotted black lines). n=15-16 technical repeats across N=3 independent biological
575 repeats. One-way ANOVA with Šidák's multiple comparisons post-test was performed on
576 biological repeats (J).
577
578 <u>Figure 3: Increased actomyosin contractility is sufficient to block mesoderm commitment and</u>
579 <u>EMT</u>

580 A – Experimental design for co-culture experiment. hiPSC were transduced with lentivector
581 expressing ROCK2^{CA} or MLCK^{CA}. Transduced cells are mVenus positive and are mixed with WT
582 mVenus-negative hiPSCs. ROCK2^{CA}/MLCK ^{CA} expression is induced by addition of Doxycycline 24h
583 prior to initiating mesoderm differentiation. Doxycycline induction was maintained during the 3
584 days of differentiation using CHIR before fixing and staining.
585 B-H – Representative MaxIP immunofluorescence for Brachyury (B), EOMES (D), Slug (F) and ZO-
586 1 (H) in Vehicle (H2O) and Doxycycline-induced ROCK2^{CA} co-culture. mVenus-positive cell
587 clusters are highlighted by an orange dotted line. Individual channels are inverted LUT. Scale bar
588 = 50 µm. For (H), magnified mVenus-positive and mVenus-negative areas are shown as insets.
589 Scale bar = 20 µm. Quantification of Brachyury (C), EOMES (E) and Slug-positive cells (G) is
590 reported as violin plot, comparing mVenus-positive vs mVenus-negative cluster in the presence
591 or absence of Doxycycline. For Brachyury, n = 7 (+ Veh) and n=15 (+ Dox) across N=3
592 independent biological repeats. For EOMES, n=9 across N=3 independent biological repeats. For
593 Slug, n=9 (+ Veh) and n=10 (+ Dox) across N=3 independent biological repeats. One-way ANOVA
594 with Tukey's multiple comparisons post-test was performed (C, E, G).
595
596 <u>Figure 4: Reduced cell contractility promotes nuclear accumulation of active β-Catenin</u>
597 A – Experiment design for treatments and cell fractionation.
598 B-C – Representative immunoblot as explained in (A). MYPT1^{CA}-NES-mNG hiPSCs were induced
599 with CHIR for 24h in the presence or absence of Doxycycline. Whole cell lysate (WCL) was
600 collected and loaded as input while cytosolic and nuclear fractions were extracted. Fraction
601 purity was probed using cytosolic (GAPDH) and nuclear (Lamin A/C) markers. Active β-catenin
602 (non-phospho S45) enrichment was probed for each fraction and α-Tubulin was used as loading
603 control. Molecular weights (M.W.) are displayed on the right side (B). Quantification of active β-
604 catenin enrichment in the cytosolic (left) and nuclear (right) fractions. N=3 independent
605 biological repeats. Mean and S.D. are displayed. One-way ANOVA with Šidák's multiple
606 comparisons post-test was performed (C).
607 D-F – Representative confocal slice and MaxIP for active non-phospho S45 β-catenin (Inverted
608 LUT) and mNeonGreen respectively. MYPT1^{CA}-NES-mNG hiPSCs were fixed at 0h and 24h post
609 CHIR treatment complemented or not with Doxycycline. Scale bar = 50 µm. Insets represent a
610 magnified view of the active non-phospho S45 β-catenin with an example of the nuclei binary

611 mask overlaid (pink). Scale bar = 10 µm (D). Schematic representation of the quantification
612 pipeline. (E). Quantification of active non-phospho S45 β-catenin mean intensity as depicted in
613 (E). n = 10-12 technical repeats across N=3 independent biological repeats. Mean and S.D. are
614 displayed. One-way ANOVA with Šidák's multiple comparisons post-test was performed (F).
615 G – Relative expression of WNT target genes (*LEF1* and *AXIN1*) with increasing concentration of
616 CHIR in the presence (Magenta) or absence (Cyan) of ROCK inhibitor Y-27632. N=7 independent
617 biological repeats. Mean and S.E.M. are displayed. One-way ANOVA with Šidák's multiple
618 comparisons post-test was performed.
619 H – Graphical abstract. Bottom right panel: Upon constitutively high contractile forces,
620 mesoderm specification is strongly inhibited. Bottom right panel: Cell relaxation promotes
621 mesoderm conversion by driving accumulation of nuclear β-catenin and licensing of WNT
622 pathway signaling.
623
624 <u>Supplementary Figure 1: hiPSC differentiation along the cardiac mesoderm increases</u>
625 <u>actomyosin-driven contractility (Related to Figure 1)</u>
626 A – Bright field imaging of WT hiPSCs treated with CHIR in the presence or absence of a pan-
627 Caspase inhibitor Q-VD-OPH. Retraction area is highlighted in yellow. Time is presented as
628 hh:mm. Scale bar = 20 µm.
629 B, C – Confocal XZ orthogonal views (B) and Maximum Intensity Projections (MaxIP) (C) of
630 hiPSCs at basal state (0h CHIR) or post-CHIR treatment (24h and 48h CHIR), stained for DNA
631 (Cyan) and F-Actin (Grey). Scale bar = 10 µm.
632 D – Quantification of the monolayer height at 0h, 24h and 48h post CHIR treatment from (B).
633 Violin plots represent individual measurements (small dots) averaged for each biological repeat
634 (large dots). Median (Plain red line) and quartiles (Dotted black lines). n=32 technical repeats
635 across N=7 independent biological repeats. A Kruskal-Wallis test with Dunn's multiple
636 comparison post-test was performed on biological repeats.
637 E, F – Representative MaxIP immunofluorescence of WT hiPSC during CHIR treatment. Fixed
638 cells were stained for DNA marker (Hoechst). Scale bar = 20 µm (E). Quantification of average
639 nuclear size from n=15 fields of view across N=3 independent biological repeats. Median (Plain
640 red line) and quartiles (Dotted black lines) are displayed. Two-tailed unpaired t test was
641 performed (F).

642 G – Correlation of cell area over cell density for each field of view during CHIR treatment.
643 Biological repeats are color-coded. Pearson correlation coefficient is displayed.
644 H – Representative MaxIP immunofluorescence of hiPSCs at basal state (0h) or post-CHIR
645 treatment (24 and 48h) stained for phospho T18/S19 MLC2 (ppMLC2). Pixels are color-coded by
646 intensity using the fire LUT.
647 I – Percentage of total imaged area that is ppMLC2-positive at 0h, 24h, 48h post CHIR is
648 reported as violin plots. Median (Plain red line) and quartiles (Dotted black lines). n=15
649 technical repeats across N=3 independent biological repeats. A Kruskal-Wallis test with Dunn's
650 multiple comparison post-test was performed on the technical repeats.
651 J – Retardance measurements obtained from hiPSCs at basal state (0h), post-CHIR treatment
652 (24h, 48h, 72h) or treated with Y-27632 at 0h (Y-27) using Quantitative Polarization Microscopy
653 imaging. Median (Plain red line) and quartiles (Dotted black lines). n=240 technical repeats for
654 0h, 24h, 48h, 72h and n=120 technical repeats for Y-27 across N=3 independent biological
655 repeats. A one-way ANOVA with Šidák's multiple comparisons post-test was performed on the
656 biological repeats.
657
658 Supplementary Figure 2: Pharmaceutical inhibition of actomyosin contractility promotes hiPSc
659 and hESC conversion to the mesoderm lineage (Related to Figure 2)
660 A, B - Representative MaxIP immunofluorescences of hiPSCs treated with a ROCK inhibitor (Y-
661 27632) or Vehicle (H_2O) and stained for nuclei marker (DNA) and phospho T18/S19 Myosin Light
662 Chain 2 (ppMLC2 – Inverted LUT). Scale bar = 50 µm. Magnified views of the yellow dotted ROI
663 are shown for ppMLC2. Scale bar = 20 µm (A). Fraction of the cellular area positive for ppMLC2
664 following Y-27632 treatment and reported as violin pots. Median (Plain red line) and quartiles
665 (Dotted black lines). n=30 technical repeats across N=3 independent biological repeats. Two-
666 tailed unpaired t test was performed on the biological repeats (B).
667 C – Relative expression of unrelated genes 48h post CHIR treatment in the presence (+Y-27) or
668 absence (+Veh) of ROCK inhibitor. N=4 independent biological repeats. Mean and S.D. are
669 displayed. Two-tailed unpaired t test was performed.
670 D - Representative MaxIP immunofluorescences of hiPSC treated 48h with CHIR in the presence
671 (+ Y-27632) or absence (+ Veh) of ROCK inhibitor. Cells were stained for nuclei marker (DNA),
672 EMT markers (ZO-1 and Slug – Inverted LUT). Scale bar = 50 µm.

673 E, F - Representative MaxIP immunofluorescences of hiPSCs treated with a ROCK inhibitor (H-
674 1152) or Vehicle (H_2O) and stained for nuclei marker (DNA) and phospho T18/S19 Myosin Light
675 Chain 2 (ppMLC2 – Inverted LUT). Scale bar = 50 µm. Magnified views of the yellow dotted ROI
676 are shown for ppMLC2. Scale bar = 20 µm (E). Fraction of the cellular area positive for ppMLC2
677 following H-1152 treatment and reported as violin pots. Median (Plain red line) and quartiles
678 (Dotted black lines). n=15 technical repeats across N=3 independent biological repeats. Two-
679 tailed unpaired t test was performed on the biological repeats (F).
680 G-K - Relative expression of mesoderm markers (*TBXT*, *MESP1, TBX6*) (G-I) and EMT markers
681 (*SNAI1, SNAI2*) (J, K) 48h post CHIR treatment in the presence (+H-1152) or absence (+Veh) of
682 ROCK inhibitor. N=3 independent biological repeats. Mean and S.D. are displayed. Two-tailed
683 unpaired t test was performed.
684 L – Immunoblot probing for mesoderm marker expression (T/Bra) and cell death marker (PARP
685 cleavage) during hiPSC-to-mesoderm commitment (0h-48h CHIR) in the presence of ROCK
686 inhibitor (+H-1152). Addition of the pan-caspases inhibitor Q-VD-OPH (+ Q-VD) to the
687 differentiation medium totally blocks mesoderm commitment and was used as negative control.
688 α-Tubulin was used as loading control. Molecular weights (M.W.) are displayed on the right side.
689 M – Representative MaxIP immunofluorescences for mesoderm marker Brachyury (T/Bra –
690 Inverted LUT) and nuclei. Cells were fixed 24h post-CHIR treatment in the presence or absence
691 of ROCK inhibitor H-1152.
692 N-P – Representative immunoblot of PARP (cell death), T/Bra (mesoderm), Oct4 and Nanog
693 (Pluripotency markers) using hESC H9 in the presence (+ Y-27632) or absence (+ Veh) of ROCK
694 inhibitor. Molecular weights (M.W.) are displayed on the right side (N). PARP cleavage (O) and
695 Nanog expression (P) was quantified by densitometry and normalized to α-Tubulin as loading
696 control across N=4 (PARP) and N=3 (Nanog) independent biological repeats. Mean and S.D. are
697 displayed. Two-tailed unpaired t test was performed.
698
699 <u>Supplementary Figure 3: Increased actomyosin contractility is sufficient to block mesoderm</u>
700 <u>commitment and EMT (Related to Figure 3)</u>
701 A – Representative MaxIP immunofluorescence of Doxycycline-induced ROCK2^{CA} hiPSCs
702 (mVenus-positive) mixed with WT hiPSCs (mVenus-negative). Cells were stained for DNA
703 (Nuclei), F-actin (top – Inverted LUT) and phospho T18/S19 Myosin Light Chain 2 (Bottom -

704 ppMLC2 – Inverted LUT). Scale bar = 50 µm. Magnified views comparing mVenus-positive
705 (Green dotted ROI) and mVenus-negative (Black dotted ROI) areas are shown for F-Actin and
706 ppMLC2. Scale bar = 10 µm.
707 B – Percentage of the ROI area positive for mVenus based on cluster considered as mVenus-
708 Negative and Positive using the ROCK2^{CA} line. On average, mVenus negative clusters have <15%
709 of their area positive for mVenus. Mean and S.E.M are displayed. n=7 (no Dox) and n=15 fields
710 of view (+Dox) across N=3 independent biological experiments.
711 C – Representative MaxIP immunofluorescence of Doxycycline-induced MLCK^{CA} hiPSCs (mVenus-
712 positive) mixed with WT hiPSCs (mVenus-negative). Cells were stained for DNA (Nuclei), F-actin
713 (top – Inverted LUT) and phospho T18/S19 Myosin Light Chain 2 (Bottom - ppMLC2 – Inverted
714 LUT). Scale bar = 50 µm. Magnified views comparing mVenus-positive (Green dotted ROI) and
715 mVenus-negative (Black dotted ROI) areas are shown for F-Actin and ppMLC2. Scale bar = 10
716 µm.
717 D – Percentage of the ROI area positive for mVenus based on cluster considered as mVenus-
718 Negative and Positive using the MLCK^{CA} line. On average, mVenus negative clusters have <15%
719 of their area positive for mVenus. Mean and S.E.M are displayed. n=7 (no Dox) and n=18 fields
720 of view (+Dox) across N=3 independent biological experiments.
721 E, F - Representative MaxIP immunofluorescence for Brachyury in Vehicle (+Veh) and
722 Doxycycline-induced MLCK^{CA} co-culture. mVenus-positive cell clusters are highlighted by an
723 orange dotted line. Individual channels are inverted LUT. Scale bar = 50 µm (E). Percentage of
724 Brachyury-positive nuclei is reported as violin plot, comparing mVenus-positive vs mVenus-
725 negative cluster in the presence or absence of Doxycycline. Median (Plain red line) and quartiles
726 (Dotted black lines). n=7 (+Veh) and n=18 (+ Dox) fields of view (small dots) across N=3
727 independent biological repeats (large dots). One-way ANOVA with Tukey's multiple comparisons
728 post-test was performed (F).
729 G - Representative MaxIP immunofluorescence for EOMES, Slug and ZO-1 in Doxycycline-
730 induced MLCK^{CA} co-culture. mVenus-positive cell clusters are highlighted by an orange dotted
731 line. Individual channels are inverted LUT. Scale bar = 50 µm.
732
733 <u>Supplementary Figure 4: Reduced cell contractility promotes nuclear accumulation of active β-</u>
734 <u>catenin (Related to Fig. 4)</u>

735 A, B – Immunoblot for phospho S127 YAP (pYAP)and total YAP following differentiation (0-48h
736 CHIR) in the presence or absence of ROCK inhibitor Y-27632. Brachyury expression was also
737 probed as an internal positive control and α-Tubulin was used as loading control. Molecular
738 weights (M.W.) are displayed on the right side (A). Ratio of phospho/total YAP was quantified
739 across N=4 independent biological repeats. Mean and S.D. are displayed. One-way ANOVA with
740 Šidák's multiple comparisons post-test was performed.
741 C – Relative expression of YAP-target genes *CTGF* and *CYR61* during differentiation in the
742 presence or absence of ROCK inhibitor Y-27632. N=4 independent biological repeats. Mean and
743 S.D. are displayed. One-way ANOVA with Šidák's multiple comparisons post-test was performed.
744 D - Relative expression of canonical WNT (*WNT3A, WNT8A*), non-canonical WNT (*WNT4*) and
745 mesoderm marker (*TBX6*) in MYPT1^{CA}-NES-mNG cells treated with CHIR (0-48h) in the presence
746 of Vehicle or Doxycycline. N=3 independent biological repeats. Mean and S.D. are displayed.
747 One-way ANOVA with Šidák's multiple comparisons post-test was performed.
748 E – Relative expression of *TBX6* and *MESP1* (mesoderm markers) following CHIR treatment in
749 the presence of Y-27632 complemented or not with 7.5 µM Porcupine inhibitor (IWP-2 or DMSO
750 respectively). N=3 independent biological repeats. Mean and S.D. are displayed. One-way
751 ANOVA with Tukey's multiple comparisons post-test was performed.
752 F – Compartment purity following fractionation was assessed by quantifying Lamin A/C and
753 GAPDH enrichment in both, cytosolic and nuclear fractions across N=4 independent biological
754 repeats.
755 G, H – Still pictures from confocal timelapse imaging of mEGFP-β-catenin knock-in hiPSCs
756 treated with CHIR +/- Y-26732. Time is shown in hours. Scale bar = 10 µm (G). mEGFP-β-catenin
757 intensity is reported as a scan line plot across a cell at 0h and 20h (H).
758
759 **References**
760

761 1. Firmin, J. *et al*. Mechanics of human embryo compaction. *Nature* **629**, 646–651
762 (2024).
763 2. Deglincerti, A. *et al*. Self-organization of human embryonic stem cells on
764 micropatterns. *Nat Protoc* **11**, 2223–2232 (2016).
765 3. Muncie, J. M. *et al*. Mechanical Tension Promotes Formation of Gastrulation-like
766 Nodes and Patterns Mesoderm Specification in Human Embryonic Stem Cells. *Dev*
767 *Cell* **55**, 679-694.e11 (2020).

4. Hookway, C. *et al.* A human induced pluripotent stem (hiPS) cell model for the holistic study of epithelial to mesenchymal transitions (EMTs). *BioRxiv* (2024).
5. Fort, L., Gama, V. & Macara, I. G. Stem cell conversion to the cardiac lineage requires nucleotide signalling from apoptosing cells. *Nat Cell Biol* **24**, 434–447 (2022).
6. Lomakin, A. J. *et al.* The nucleus acts as a ruler tailoring cell responses to spatial constraints. *Science (1979)* **370**, (2020).
7. de Leeuw, N. F., Budhathoki, R., Russell, L. J., Loerke, D. & Blankenship, J. T. Nuclei as mechanical bumpers during epithelial remodeling. *Journal of Cell Biology* **223**, (2024).
8. Totsukawa, G. *et al.* Distinct roles of ROCK (Rho-kinase) and MLCK in spatial regulation of MLC phosphorylation for assembly of stress fibers and focal adhesions in 3T3 fibroblasts. *J Cell Biol* **150**, 797–806 (2000).
9. Shi, Y., Ohler, L. S., de Jesus, B. N. & Dickinson, D. J. Opposing actomyosin pools generate cortical flows that establish epithelial polarity. *Biorxiv* (2024).
10. Makishima, M. *et al.* Induction of differentiation of human leukemia cells by inhibitors of myosin light chain kinase. *FEBS Lett* **287**, 175–177 (1991).
11. Matsumura, F., Yamakita, Y. & Yamashiro, S. Myosin Phosphatase-targeting Subunit 1 Controls Chromatid Segregation. *Journal of Biological Chemistry* **286**, 10825–10833 (2011).
12. Kiss, A., Erdődi, F. & Lontay, B. Myosin phosphatase: Unexpected functions of a long-known enzyme. *Biochimica et Biophysica Acta (BBA) - Molecular Cell Research* **1866**, 2–15 (2019).
13. Yamamoto, K. *et al.* Optogenetic relaxation of actomyosin contractility uncovers mechanistic roles of cortical tension during cytokinesis. *Nat Commun* **12**, 7145 (2021).
14. Stronati, E. *et al.* YAP1 regulates the self-organized fate patterning of hESC-derived gastruloids. *Stem Cell Reports* **17**, 211–220 (2022).
15. Röper, J.-C. *et al.* The major β-catenin/E-cadherin junctional binding site is a primary molecular mechano-transductor of differentiation in vivo. *Elife* **7**, (2018).
16. van der Wal, T. & van Amerongen, R. Walking the tight wire between cell adhesion and WNT signalling: a balancing act for β-catenin. *Open Biol* **10**, (2020).
17. Orsulic, S., Huber, O., Aberle, H., Arnold, S. & Kemler, R. E-cadherin binding prevents β-catenin nuclear localization and β-catenin/LEF-1-mediated transactivation. *J Cell Sci* **112**, 1237–1245 (1999).
18. Roura, S., Miravet, S., Piedra, J., de Herreros, A. G. & Duñach, M. Regulation of E-cadherin/Catenin Association by Tyrosine Phosphorylation. *Journal of Biological Chemistry* **274**, 36734–36740 (1999).
19. Gayrard, C., Bernaudin, C., Déjardin, T., Seiler, C. & Borghi, N. Src- and confinement-dependent FAK activation causes E-cadherin relaxation and β-catenin activity. *Journal of Cell Biology* **217**, 1063–1077 (2018).
20. Brunet, T. *et al.* Evolutionary conservation of early mesoderm specification by mechanotransduction in Bilateria. *Nat Commun* **4**, 2821 (2013).
21. Llewellyn, J., Charrier, A., Cuciniello, R., Helfer, E. & Dono, R. Substrate stiffness alters layer architecture and biophysics of human induced pluripotent stem cells to modulate their differentiation potential. *iScience* **27**, 110557 (2024).
22. Maldonado, M., Luu, R. J., Ramos, M. E. P. & Nam, J. ROCK inhibitor primes human induced pluripotent stem cells to selectively differentiate towards mesendodermal

lineage via epithelial-mesenchymal transition-like modulation. *Stem Cell Res* **17**, 222–227 (2016).

23. Kashkooli, L., Rozema, D., Espejo-Ramirez, L., Lasko, P. & Fagotto, F. Ectoderm to mesoderm transition by down-regulation of actomyosin contractility. *PLoS Biol* **19**, e3001060 (2021).
24. Lian, X. *et al.* Robust cardiomyocyte differentiation from human pluripotent stem cells via temporal modulation of canonical Wnt signaling. *Proceedings of the National Academy of Sciences* **109**, (2012).
25. Lian, X. *et al.* Directed cardiomyocyte differentiation from human pluripotent stem cells by modulating Wnt/β-catenin signaling under fully defined conditions. *Nat Protoc* **8**, 162–175 (2013).
26. Vasic, I. *et al.* Loss of TJP1 disrupts gastrulation patterning and increases differentiation toward the germ cell lineage in human pluripotent stem cells. *Dev Cell* **58**, 1477-1488.e5 (2023).
27. Dupont, S. *et al.* Role of YAP/TAZ in mechanotransduction. *Nature* **474**, 179–183 (2011).
28. Pagliari, S. *et al.* YAP–TEAD1 control of cytoskeleton dynamics and intracellular tension guides human pluripotent stem cell mesoderm specification. *Cell Death Differ* **28**, 1193–1207 (2021).
29. Leptin, M. & Grunewald, B. Cell shape changes during gastrulation in *Drosophila*. *Development* **110**, 73–84 (1990).
30. Skory, R. M. *et al.* The nuclear lamina couples mechanical forces to cell fate in the preimplantation embryo via actin organization. *Nat Commun* **14**, 3101 (2023).
31. Caldarelli, P. *et al.* Self-organized tissue mechanics underlie embryonic regulation. *Nature* **633**, 887–894 (2024).
32. Rozbicki, E. *et al.* Myosin-II-mediated cell shape changes and cell intercalation contribute to primitive streak formation. *Nat Cell Biol* **17**, 397–408 (2015).
33. Dahl, K. N., Kahn, S. M., Wilson, K. L. & Discher, D. E. The nuclear envelope lamina network has elasticity and a compressibility limit suggestive of a molecular shock absorber. *J Cell Sci* **117**, 4779–4786 (2004).
34. Maître, J.-L. *et al.* Adhesion Functions in Cell Sorting by Mechanically Coupling the Cortices of Adhering Cells. *Science (1979)* **338**, 253–256 (2012).
35. Krieg, M. *et al.* Tensile forces govern germ-layer organization in zebrafish. *Nat Cell Biol* **10**, 429–436 (2008).
36. Turlier, H. & Maître, J.-L. Mechanics of tissue compaction. *Semin Cell Dev Biol* **47–48**, 110–117 (2015).
37. Loza, A. J. *et al.* Cell density and actomyosin contractility control the organization of migrating collectives within an epithelium. *Mol Biol Cell* **27**, 3459–3470 (2016).
38. Yamaguchi, T. P., Takada, S., Yoshikawa, Y., Wu, N. & McMahon, A. P. T (Brachyury) is a direct target of Wnt3a during paraxial mesoderm specification. *Genes Dev* **13**, 3185–3190 (1999).
39. Arnold, S. J. *et al.* Brachyury is a target gene of the Wnt/β-catenin signaling pathway. *Mech Dev* **91**, 249–258 (2000).

Figure 1

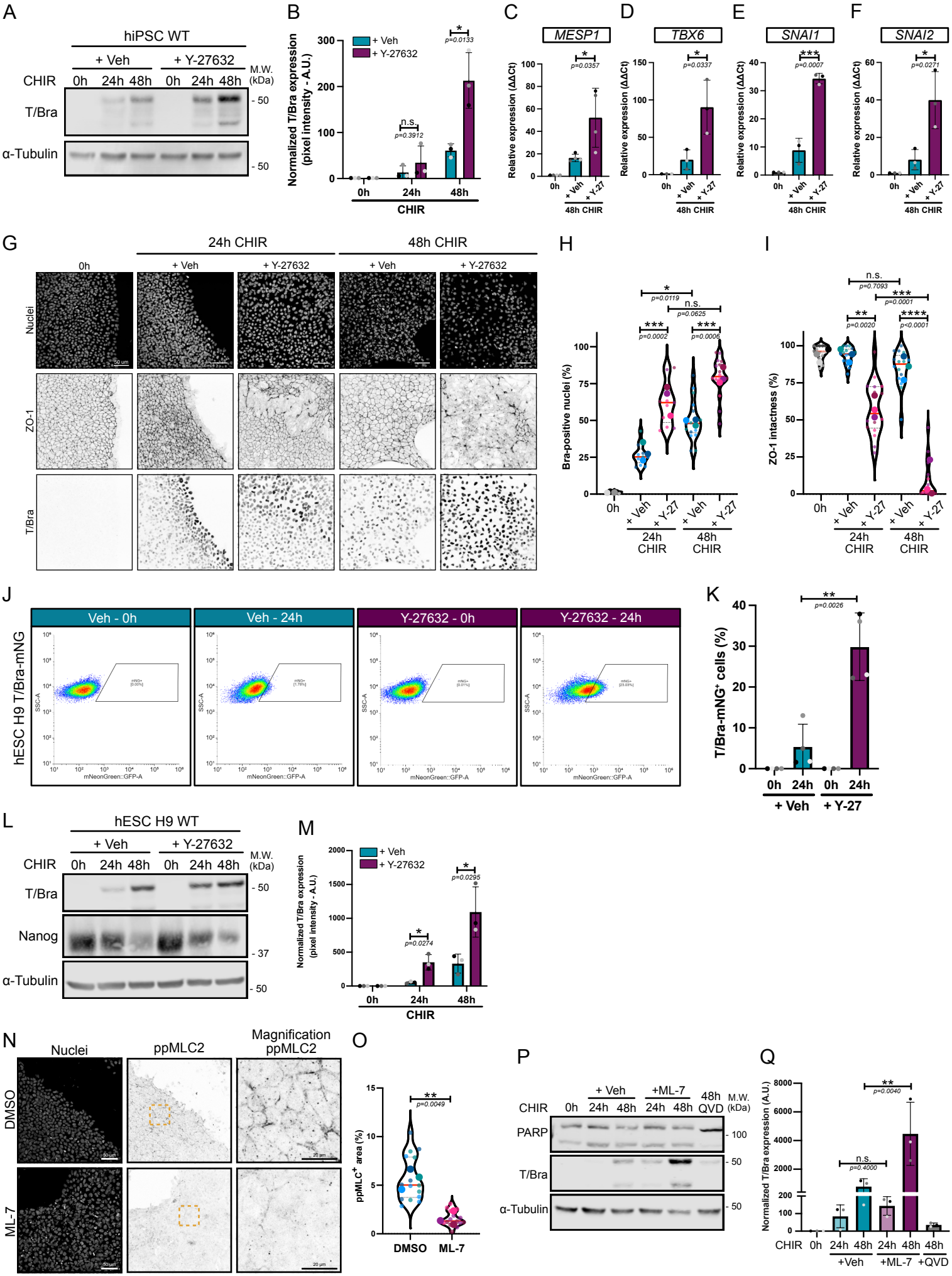
A
hiPSC WT
+ Veh
+ Y-27632
CHIR
0h 24h 48h 0h 24h 48h
M.W. (kDa)
T/Bra
α-Tubulin
- 50
- 50
B
Normalized T/Bra expression (pixel intensity - A.U.)
+ Veh
+ Y-27632
n.s. p=0.3912
* p=0.0133
0h 24h 48h
CHIR
C
MESP1
* p=0.0357
D
TBX6
* p=0.0337
E
SNAI1
*** p=0.0007
F
SNAI2
* p=0.0271
Relative expression (ΔΔCt)
0h
+ Veh
+ Y-27
48h CHIR
G
24h CHIR
48h CHIR
0h
+ Veh
+ Y-27632
Nuclei
ZO-1
T/Bra
H
Bra-positive nuclei (%)
* p=0.0119
n.s. p=0.0625
*** p=0.0002
*** p=0.0006
24h CHIR
48h CHIR
I
ZO-1 intactness (%)
n.s. p=0.7093
*** p=0.0001
** p=0.0020
**** p<0.0001
J
hESC H9 T/Bra-mNG
Veh - 0h
Veh - 24h
Y-27632 - 0h
Y-27632 - 24h
mNeonGreen::GFP-A
SSC-A
K
T/Bra-mNG+ cells (%)
** p=0.0026
0h 24h 0h 24h
+ Veh + Y-27
L
hESC H9 WT
+ Veh
+ Y-27632
CHIR
0h 24h 48h 0h 24h 48h
M.W. (kDa)
T/Bra
Nanog
α-Tubulin
- 50
- 37
- 50
M
Normalized T/Bra expression (pixel intensity - A.U.)
+ Veh
+ Y-27632
* p=0.0274
* p=0.0295
0h 24h 48h
CHIR
N
Nuclei
ppMLC2
Magnification ppMLC2
DMSO
ML-7
O
ppMLC+ area (%)
** p=0.0049
DMSO ML-7
P
CHIR
0h 24h 48h 24h 48h 48h QVD
+ Veh
+ ML-7
M.W. (kDa)
PARP
T/Bra
α-Tubulin
- 100
- 50
- 50
Q
Normalized T/Bra expression (A.U.)
** p=0.0040
n.s. p=0.4000
CHIR 0h 24h 48h 24h 48h 48h
+Veh +ML-7 +QVD

Figure 2

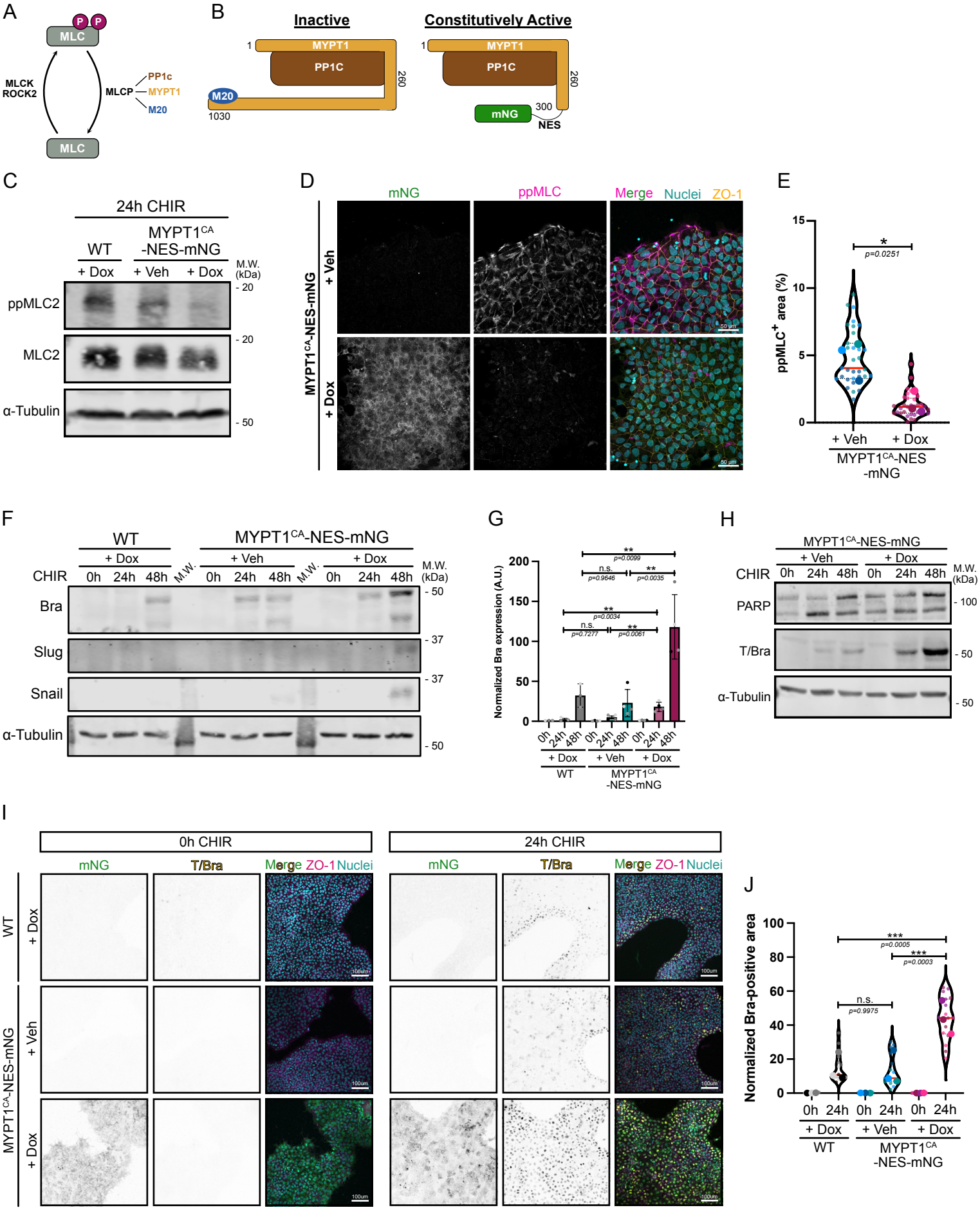
A
MLC
P
P
MLCK
ROCK2
MLCP
PP1c
MYPT1
M20
MLC
B
Inactive
Constitutively Active
MYPT1
PP1C
M20
1
1030
260
mNG
300
NES
C
24h CHIR
WT
MYPT1CA -NES-mNG
+ Dox
+ Veh
+ Dox
M.W. (kDa)
ppMLC2
MLC2
α-Tubulin
- 20
- 20
- 50
D
mNG
ppMLC
Merge
Nuclei
ZO-1
MYPT1CA-NES-mNG
+ Veh
+ Dox
E
ppMLC+ area (%)
p=0.0251
+ Veh
+ Dox
MYPT1CA-NES -mNG
F
WT
MYPT1CA-NES-mNG
CHIR
0h
24h
48h
M.W.
Bra
Slug
Snail
α-Tubulin
- 50
- 37
- 37
- 50
G
Normalized Bra expression (A.U.)
p=0.0099
n.s.
p=0.9646
p=0.0035
p=0.0034
n.s.
p=0.7277
p=0.0061
WT
MYPT1CA -NES-mNG
H
MYPT1CA-NES-mNG
PARP
T/Bra
α-Tubulin
- 100
- 50
- 50
I
0h CHIR
24h CHIR
mNG
T/Bra
Merge ZO-1 Nuclei
WT
MYPT1CA-NES-mNG
+ Dox
+ Veh
+ Dox
J
Normalized Bra-positive area
p=0.0005
p=0.0003
n.s.
p=0.9975
WT
MYPT1CA -NES-mNG

Figure 3

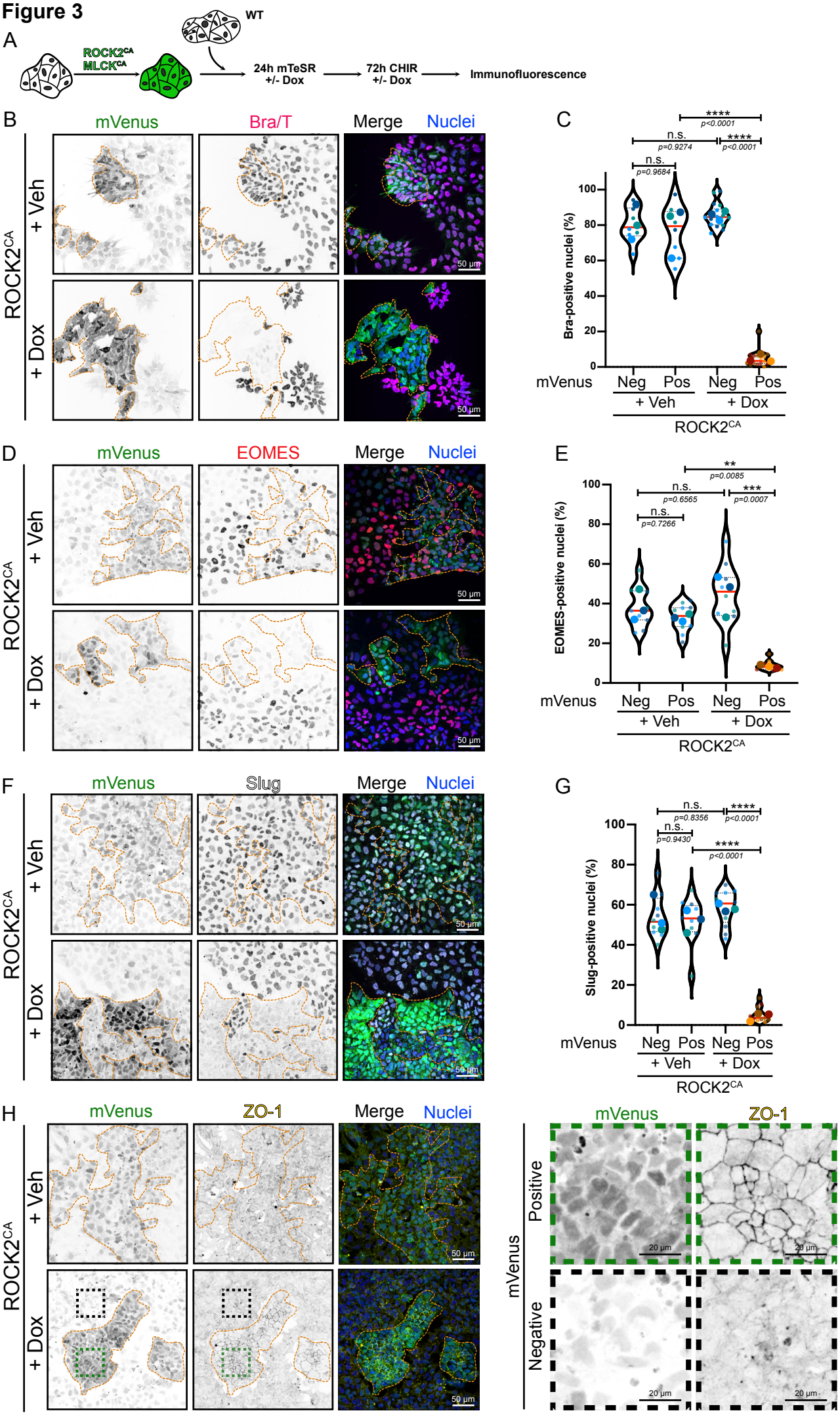
A
ROCK2CA
MLCKCA
WT
24h mTeSR
+/- Dox
72h CHIR
+/- Dox
Immunofluorescence
B
mVenus
Bra/T
Merge
Nuclei
ROCK2CA
+ Veh
+ Dox
50 µm
C
Bra-positive nuclei (%)
n.s.
p=0.9684
n.s.
p=0.9274
****
p<0.0001
****
p<0.0001
mVenus
Neg
Pos
Neg
Pos
+ Veh
+ Dox
ROCK2CA
D
mVenus
EOMES
Merge
Nuclei
E
EOMES-positive nuclei (%)
n.s.
p=0.7266
n.s.
p=0.6565
**
p=0.0085
***
p=0.0007
F
mVenus
Slug
Merge
Nuclei
G
Slug-positive nuclei (%)
n.s.
p=0.9430
n.s.
p=0.8356
****
p<0.0001
****
p<0.0001
H
mVenus
ZO-1
Merge
Nuclei
Positive
Negative
20 µm

Figure 4

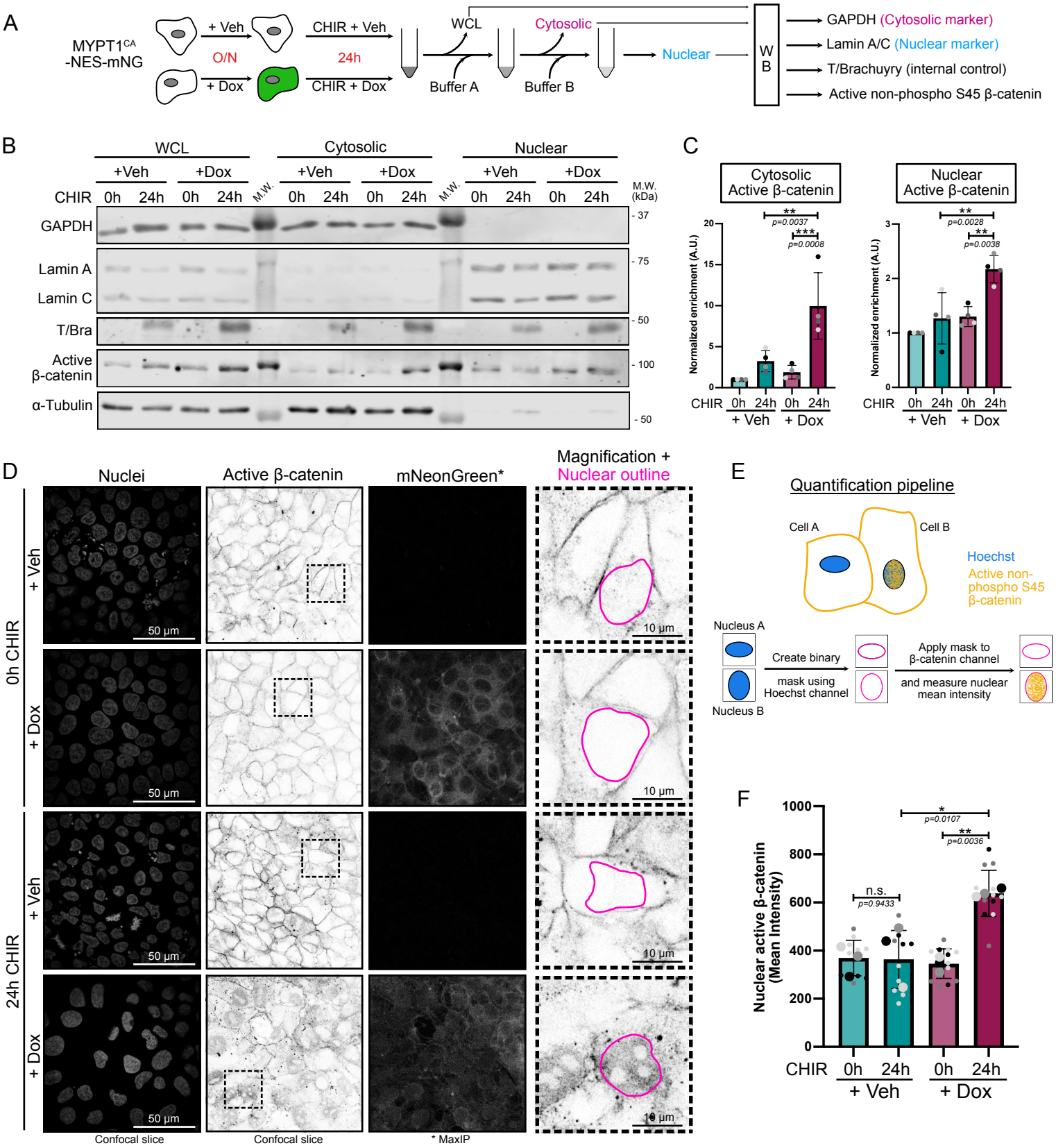
A
MYPT1CA -NES-mNG
+ Veh
O/N
+ Dox
CHIR + Veh
24h
CHIR + Dox
WCL
Buffer A
Cytosolic
Buffer B
Nuclear
WB
GAPDH (Cytosolic marker)
Lamin A/C (Nuclear marker)
T/Brachuyry (internal control)
Active non-phospho S45 β-catenin
B
WCL
Cytosolic
Nuclear
+Veh
+Dox
CHIR 0h 24h 0h 24h
M.W.
M.W. (kDa)
GAPDH
Lamin A
Lamin C
T/Bra
Active β-catenin
α-Tubulin
- 37
- 75
- 50
- 100
- 50
C
Cytosolic Active β-catenin
Nuclear Active β-catenin
Normalized enrichment (A.U.)
p=0.0037
p=0.0008
p=0.0028
p=0.0038
CHIR 0h 24h 0h 24h
+ Veh + Dox
D
Nuclei
Active β-catenin
mNeonGreen*
Magnification + Nuclear outline
0h CHIR
24h CHIR
+ Veh
+ Dox
50 µm
10 µm
Confocal slice
Confocal slice
* MaxIP
E
Quantification pipeline
Cell A
Cell B
Hoechst
Active non-phospho S45 β-catenin
Nucleus A
Nucleus B
Create binary mask using Hoechst channel
Apply mask to β-catenin channel and measure nuclear mean intensity
F
Nuclear active β-catenin (Mean Intensity)
n.s.
p=0.9433
p=0.0107
p=0.0036
CHIR 0h 24h 0h 24h
+ Veh + Dox
G
LEF1
AXIN2
Normalized mRNA expression (ΔΔCt)
n.s.
p=0.4906
p=0.0234
p=0.0006
p<0.0001
p=0.0002
p=0.0496
p=0.0331
Veh Y-27 Veh Y-27 Veh Y-27
0h 7.5 µM 15 µM
24h CHIR
H
Working model
Contractility
Mesoderm identity
Nuclear β-catenin
WNT signaling

Supplementary Figure 1

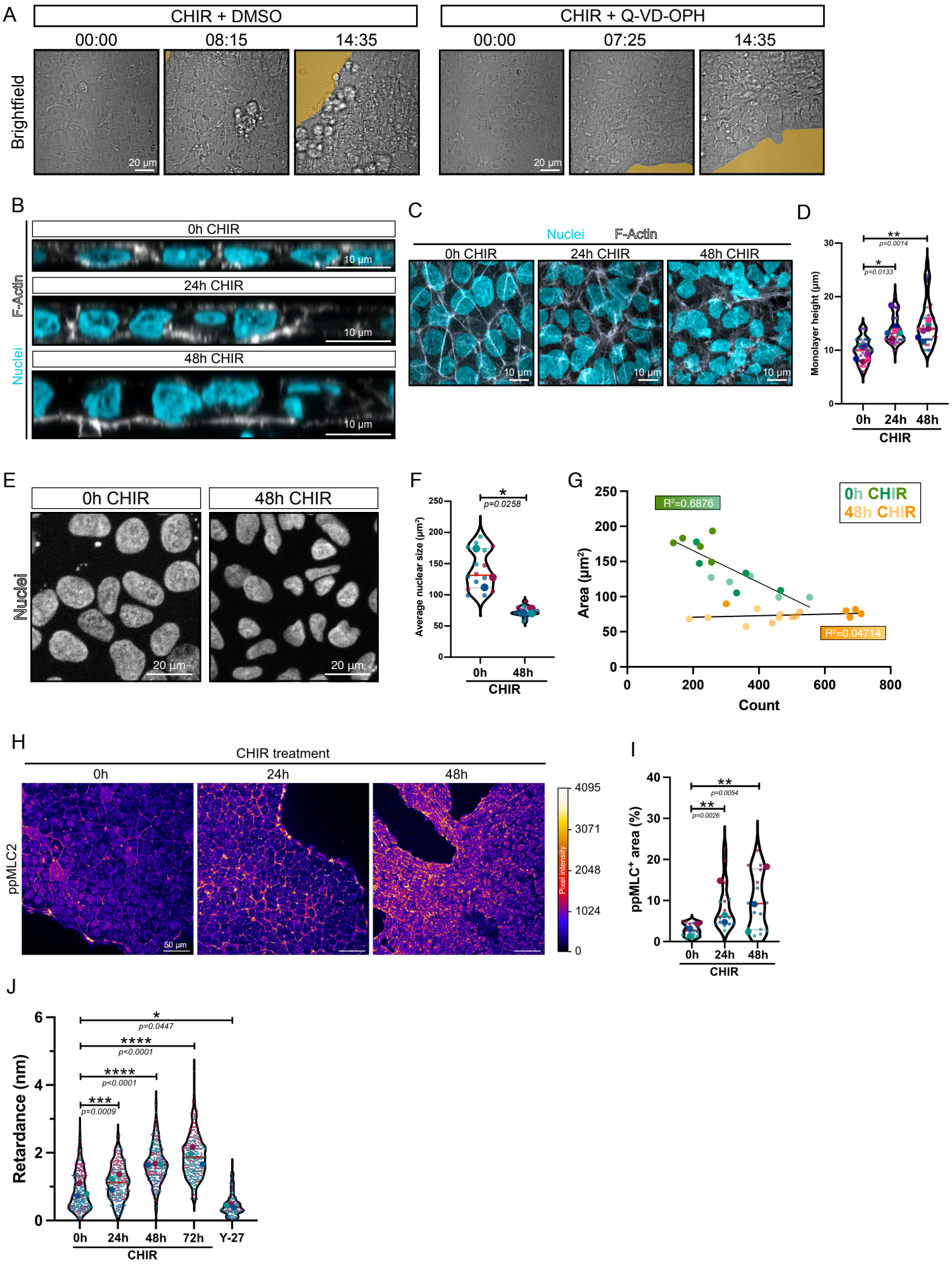

Supplementary Figure 1 (Related to Figure 2)

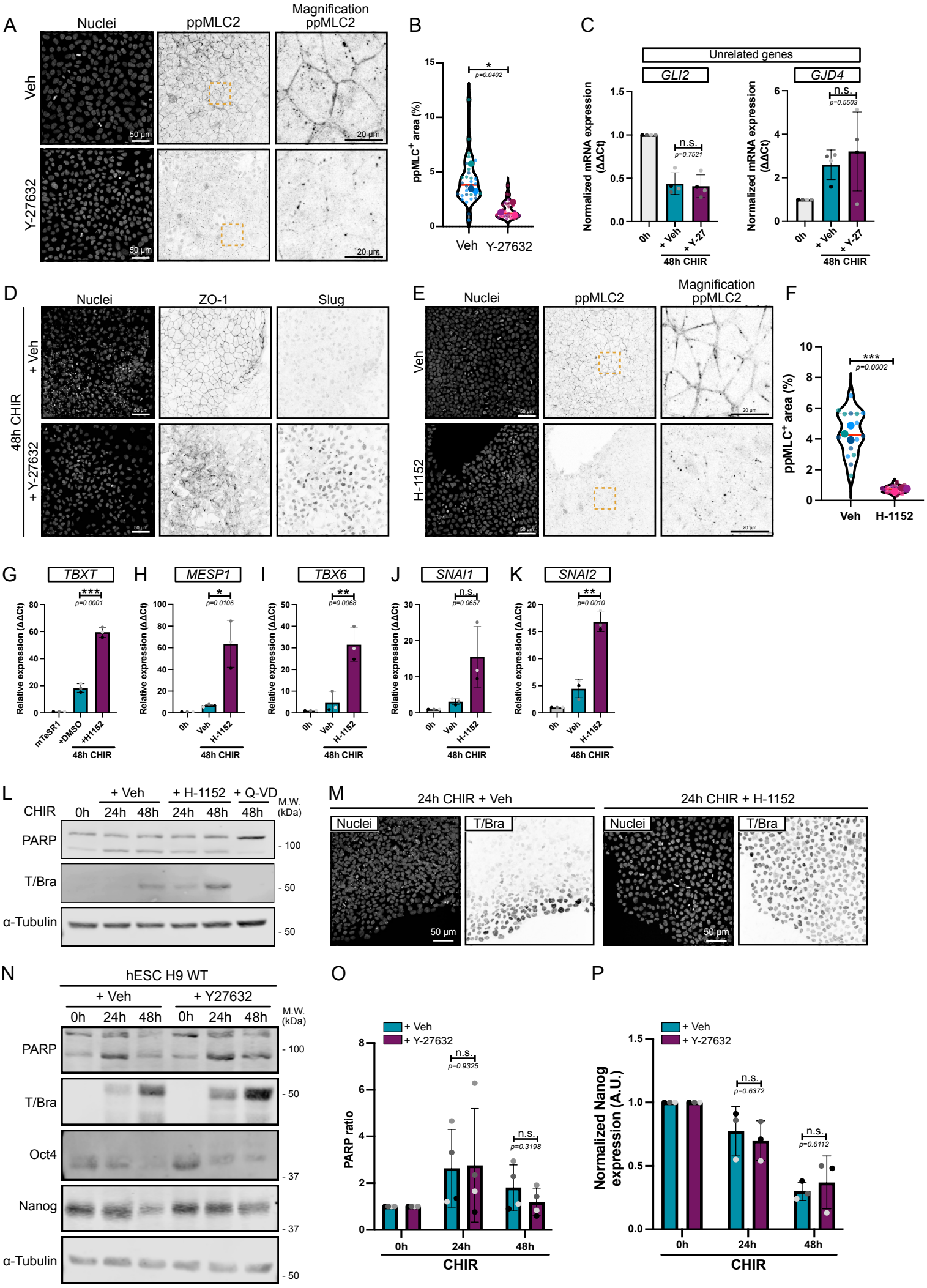

Supplementary Figure 3 (Related to Figure 3)

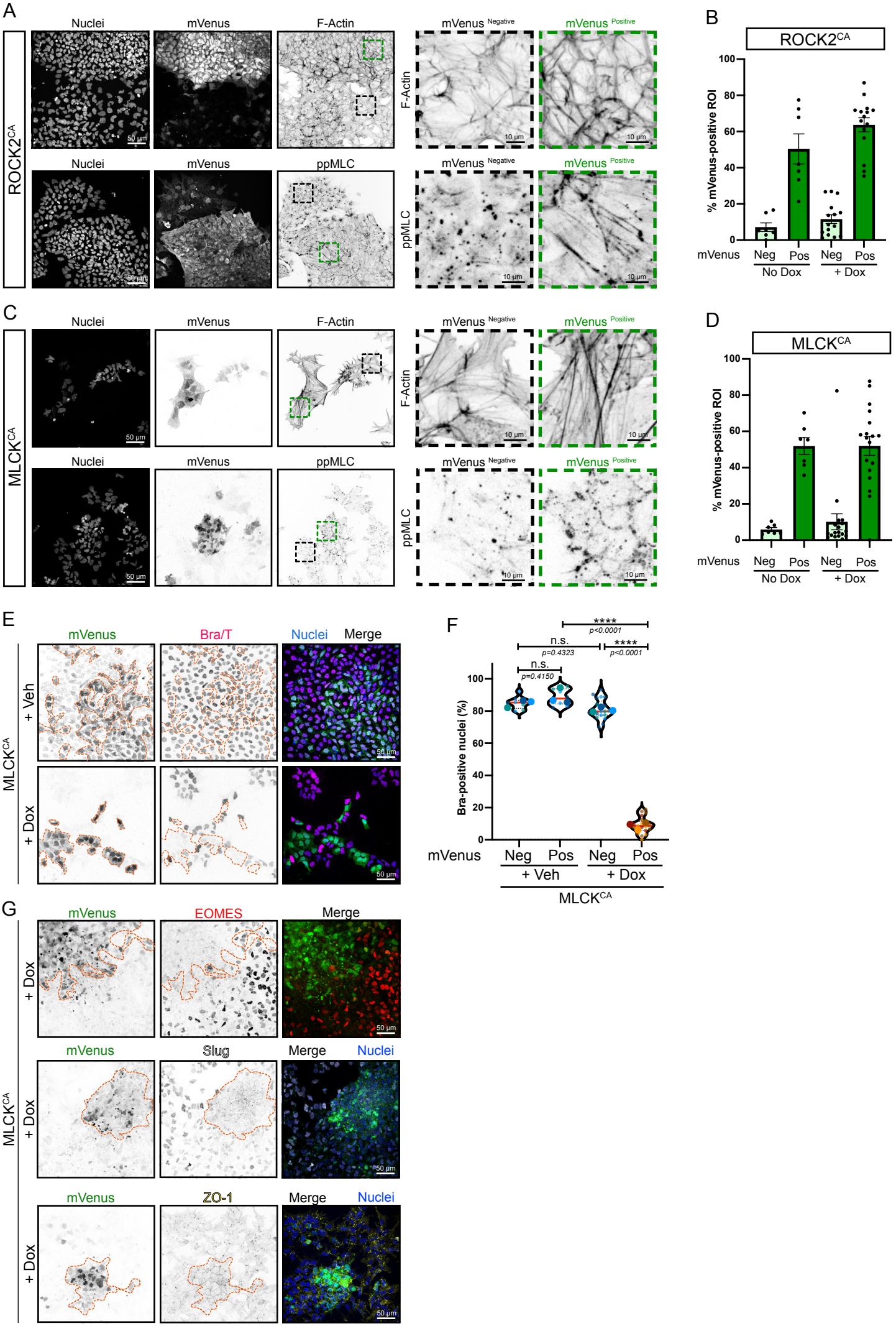
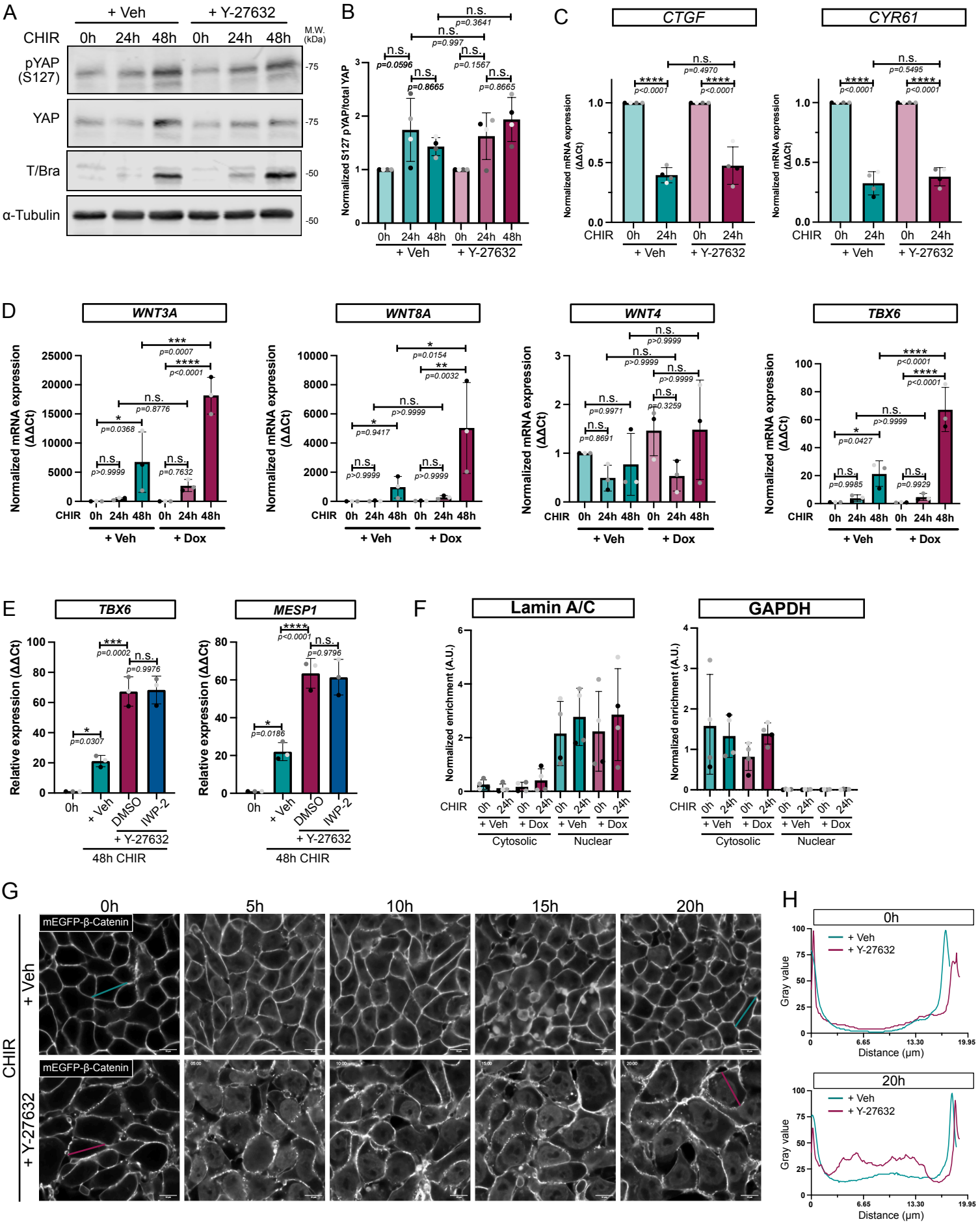
Supplementary Figure 4 (Related to Figure 4)